Diatom growth, biogenic silica production, and grazing losses to microzooplankton during spring in the northern Bering and Chukchi Seas

Jeffrey W. Krause[a,b*], Michael W. Lomas[c], Seth L. Danielson[d]

[a]Dauphin Island Sea Lab, Dauphin Island, AL, USA
[b]Department of Marine Sciences, University of South Alabama, Mobile, AL, USA
[c]Bigelow Laboratory for Ocean Sciences, East Boothbay, ME, USA
[d]College of Fisheries and Ocean Science, University of Alaska Fairbanks, Fairbanks, AK, USA

*Corresponding author
E-mail address: jkrause@disl.edu (J.W. Krause)

Keywords: diatoms, microzooplankton, biogenic silica production, dilution experiments, colimitation

Abstract

It is unclear how warming polar marine systems will alter the magnitude of diatom productivity and its fate within the food web. We examined diatom productivity and size-fractionated phytoplankton grazing losses to protozoan grazers in the northern Bering and Chukchi seas during June 2017. Sea ice was nearly absent and water temperatures were unseasonably warm; such conditions may be considered normal in future decades. Among 28 experiments conducted, five were in bloom conditions. Diatom biomass and production rates were similar to previous studies, suggesting the early ice retreat did not lead to appreciably reduced diatom growth. Statistical analyses showed that 77% of the variance in diatom growth rate could be explained by a combination of nutrients, light, and their interaction, but the interactive effect was most important (explaining 66 % of the variance). Protozoan grazing intensity on phytoplankton was largely affected by size, specifically, grazing on larger phytoplankton (e.g. diatoms) was highly variable among stations, with many stations having unquantifiable rates. Protozoan grazers consumed an average of 23 ± 35% of growth at bloom stations and 55 ± 102% among non-bloom stations. For smaller phytoplankton, grazing was persistent and less variable spatially, consuming 64 ± 38% of growth at bloom stations and 79 ± 63% at non-bloom stations. Although previous studies (that did not size-fractionate samples) inferred that protozoan grazers control diatom biomass during blooms, our results suggest that diatom productivity largely escaped protozoan grazing losses, especially in bloom conditions, likely due to temporal lag between phytoplankton and protist biomass accumulation. Thus, during bloom conditions, it was estimated that 20-50 times more diatom organic matter was available for higher trophic levels

and/or export (as opposed to water column remineralization) than under non-bloom conditions, despite only a 12-fold increase in gross diatom production in the bloom.

1. Introduction

While predicting future productivity in the Bering Sea (BS) and Chukchi Sea (CS) is important, a more pressing concern in this system is determining the fate of primary production within the food web. Existing data in the BS show that annual primary productivity is higher in years with poorer survivorship of age-0 walleye pollock (*Theragra chalcogramma*)—the most important regional and global (2014 data) fishery by landings (Eisner et al., 2014; FAO, 2016; Hunt et al., 2011). The lack of a significant correlation between fisheries potential and annual primary production could imply not-direct or non-linear relationships between these rates. Indeed, the 2019 Ecosystem Status report for the eastern BS show no correlation between the annual mean abundance of large copepods and euphausiids (age-0 walleye pollock prey) and the average primary production rate during the growing season, whereas there is a positive correlation between smaller copepods (not as favorable for age-0 walleye pollock) and primary production (Kimmel et al., 2019; Nielsen et al., 2019). Such a lack of understanding limits our predictive capability to determine whether hypothetical increases in future primary production may fuel enhanced higher trophic biomass in the pelagic or benthic realms. Whether diatoms will continue to have a dominant role in regional spring productivity is also unknown. Bottom-up factors, e.g. warming, could reduce diatoms' element per unit biovolume (i.e. elemental density), and therefore reduce the quantity of carbon produced (Krause and Lomas, 2020; Lomas et al., 2019), even if other bottom-up factors (increased light, nutrient fluxes) favor faster growth rates. Understanding the fate of diatom primary production has important ramifications, from modeling changes in regional biogeochemical cycles to diagnosing whether the ecosystem will sustain economically important services.

While multiple groups of phytoplankton persist in the high-latitude Alaskan Seas, larger cells such as diatoms play key food-web roles, especially during blooms in both the spring and summer (Giesbrecht and Varela, 2021; Krause and Lomas, 2020; Yang et al., 2015). During the spring, the phytoplankton community increases biomass and fuels efficient transfer of energy and materials to higher trophic levels; under such conditions diatoms dominate phytoplankton

biomass and the community rate of primary production (Baumann et al., 2014; Lomas et al., 2012). During cold-anomaly years in the eastern BS, Baumann et al. (2014) observed that diatom contribution to total phytoplankton biomass averaged 80% in the spring. A recent analysis of data from 2006 through 2016 demonstrated that warm anomaly years have higher phytoplankton biomass but the size structure is not significantly different from cool anomaly years (Lomas et al., 2020).

Microzooplankton (MZP) and larger mesozooplankton (LMZP e.g. calanoid copepods, euphausiids) are important consumers of regional phytoplankton productivity (Campbell et al., 2016; Sherr et al., 2013). Relative to most phytoplankton groups, diatoms' larger size makes them favorable food sources for LMZP, which are themselves important prey items for age-0 class walleye pollock. On the eastern BS shelf, stable isotope data suggest LMZP graze more heavily on diatoms and other primary producers than MZP (Morales et al., 2014). However, analyses based on direct feeding experiments have shown that while LMZP prefer MZP as prey, in the spring and early summer; MZP biomass is minor compared to phytoplankton, and therefore, phytoplankton dominate LMZP diets under these conditions (Campbell et al., 2016). Such direct ingestion allows for a more efficient trophic transfer of phytoplankton organic matter than "phytoplankton → MZP → LMZP" pathways (Sherr et al., 2013; Stoecker et al., 2014a; Yang et al., 2015), which compound respiration losses from the increased number of trophic steps. Thus, processing primary productivity through the microbial loop may be one of the underlying factors affecting the observed spatial variations in organic matter quality based on C:N ratios, e.g. Grebmeier et al. (1988).

Regional studies show that MZP can be a major carbon pool within the food web for higher consumers (e.g. copepods) and they can consume significant quantities of primary production. Previous studies demonstrate that MZP biomass in these systems are variable and, at times, can exceed phytoplankton biomass by multiple factors, ranging from 0.2 – 109 µg C L^{-1} during spring (Sherr et al., 2013) and 1– >150 µg C L^{-1} during summer (Olson and Strom, 2002; Stoecker et al., 2014b; Strom and Fredrickson, 2008; Yang et al., 2015). Similarly, summer studies have observed that MZP carbon can exceed phytoplankton carbon, especially when chlorophyll *a* (Chl *a*) concentrations are low. During the Bering Ecosystem Study (BEST) and Bering Sea Integrated Ecosystem Research Program (BSIERP), it was recognized that there is a seasonal increase in the relative importance of MZP grazing relative to phytoplankton growth. In

the spring, MZP grazing rates averaged 46% of phytoplankton growth among bloom and non-bloom conditions (Sherr et al., 2013). Farther north, in the CS and Beaufort Sea during late spring and early summer (Shelf–Basin Interactions program), Sherr et al. (2009) observed that MZP grazing consumed between 0–120% of daily primary production (note: >100% losses of daily primary production reduces phytoplankton standing stock), with an average of 22% —approximately half the spring rates observed during BEST/BSIERP. More recent results demonstrated similar variability in the CS during spring 2014, where MZP grazed 31–>100% of primary production, with an average of 46% (Connell et al., 2018). While these data demonstrate that MZP can be an important control on total phytoplankton biomass and productivity, size-fractionated data for the BS are only reported for the summer (Olson and Strom, 2002; Strom and Fredrickson, 2008). During summer in the Chukchi, Yang et al. (2015) directly quantified diatom losses to MZP (based on cell counts), and showed it was substantial (63% ± 21% SD of diatom production); however, whether this is similar in the spring is unknown. The lack of size-fractionated data during spring precludes us from understanding which phytoplankton size classes are being controlled by MZP. Sherr et al. (2013) note that the disparity in growth rates between MZP and diatoms during early bloom stages in the BS is due to the lag of MZP growth rate to availability of phytoplankton prey (i.e. MZP growth approaches maximum rates at high prey biomass levels). This disparity during spring suggests that regional diatoms could grow (at times) with minor losses due to MZP. Such a condition would enable a high proportion of diatom carbon being directly consumed by higher trophic level organisms (e.g. LMZP, larval fish) and/or exported to the benthos via sedimentation (e.g. single cell sinking, association with aggregates).

In this study, we report rates of diatom growth and productivity, along with rates for MZP grazing on both large (≥5 µm) and small (<5 µm) phytoplankton during spring in the northern BS and CS during a year experiencing early-ice retreat and anomalously warm temperatures (Baker et al., 2020; Walsh et al., 2018). The grazing measurements are coupled to measurements of diatom productivity using a silicon tracer method, as diatoms are the only major phytoplankton group having an obligate silicon requirement. Such early-ice retreat conditions may affect regional food web phenology by altering when the main phytoplankton bloom occurs and the growth/success of consumers which require this production pulse. Given the projected warming trends through the end of the 21st century for the pan-Arctic region (IPCC,

2014) and the potential for ecological reordering in this region (Huntington et al., 2020), understanding the proportion of primary production which is consumed by MZP will be important for setting upper limits for the availability of primary production to higher trophic organisms in this system.

2. Methods

2.1. Collection and hydrography

Microzooplankton grazing, phytoplankton growth, and diatom productivity rates were measured during the Arctic Shelf Growth, Advection, Respiration and Deposition (ASGARD, Chief Scientist S. Danielson) cruise in the northern BS and CS aboard the R/V Sikuliaq from 9 – 28 June 2017 (Fig. 1). Hydrographic properties were measured using a SeaBird SBE CTD equipped with a Biospherical QSP-240 photosynthetically active radiation (PAR) meter, Wetlabs FLRTD fluorometer and SeaBird SBE 43 O_2 meter. Water was collected at two depths, based on the percent PAR relative to that just below the surface (%I_0), typically the 50%I_0 depth (upper euphotic zone) and the lower euphotic zone (5% or 1%I_0). One Niskin bottle per depth was sampled directly into darkened acid-cleaned 20 L carboys through a 200 µm Nitex mesh. This water was used for all rate measurements and particulate matter standing stock measurements, and the carboys were gently mixed by inversion before any subsamples were taken. Nutrient samples were collected directly from Niskin bottles taken at the same depth and syringe filtered through 0.45 µm cellulose acetate membranes and immediately frozen. On shore, silicic acid, phosphate, nitrate, nitrite and ammonium were analyzed using standard methods described by Mordy et al. (2012).

2.2. Particulate matter standing stocks

Particulate matter standing stocks were subsampled and analyzed using standard methods. After gently homogenizing the carboy, triplicate subsamples per depth were taken for measurement of Chl *a* and biogenic silica ($bSiO_2$) and a single sample was collected for diatom abundance and morphometrics. 1.0 L Chl *a* samples were filtered sequentially through 5 µm

polycarbonate membranes housed in 47 mm in-line filter holders, and glass fiber filters (0.7 µm approximate pore size) housed in 25 mm in-line filter holders. Thus, each triplicate bottle had both ≥5 and <5 µm fraction measurements. At sea, Chl *a* samples were extracted in acetone for 24 hours at -20 °C and quantified using an acidification method on a TD10-AU fluorometer calibrated at sea with a pure chlorophyll standard (Sigma–Aldrich, C6144); daily calibration checks were done using a solid standard, as in Lomas et al. (2012).

Two $bSiO_2$ metrics are reported. For total $bSiO_2$ standing stock, which includes both that associated with live cells and detrital fragments, 0.6 – 1.0 L was filtered through a 1.2 µm pore size polycarbonate filter, folded in quarters and transferred to a cryogenic vial, then frozen (-20 °C). On shore, samples were dried in a 60 °C oven, and $bSiO_2$ quantified using an alkaline digestion in Teflon tubes (Krause and Lomas, 2020). To derive $bSiO_2$ standing stock associated with only living diatoms, the total $bSiO_2$ standing stock was combined with microscopy. A single 10-mL subsample was collected per depth for diatom abundance and morphometrics and was analyzed on a VS Series benchtop FlowCam (Yokogawa Fluid Imaging Technologies; Scarborough, ME). Analysis was done on unfixed samples in autoimage mode with a 10x objective and 200 µm flow cell. Given the analytical configuration, runs typically lasted ~30 minutes and samples were analyzed <2 hours post hydrocast. Diatom images (empty frustules excluded) were manually classified within the generated image files. Biovolume is among the automatically calculated morphometric properties for each imaged particle using either prolate sphere, sphere, or cylindrical shapes; for this analysis, we used only cylinder-based biovolume. As discussed in Krause and Lomas (2020), the FlowCam software assigns a single biovolume value to chains and the biovolume assignments for diatom chains are conservative, especially for longer chains. Diatom biovolume for each manually-classified image was converted to $bSiO_2$ standing stock using the cold-water diatom allometric equation for Si vs. biovolume in stationary growth (assuming most populations will not be in exponential phase at the time of sampling) reported by Lomas et al. (2019):

$$\text{Log Si (pmol cell}^{-1}) = 0.72\ (\text{Log Biovolume, } \mu m^3) - 1.34$$

This relationship was empirically determined using 11 diatom cultures grown at 2 °C. Some of these clones were isolated in lower latitudes (e.g. 40 – 59 °N) when ambient temperature was ≤3 °C. Single-cell $bSiO_2$ content was calculated and the summation of all imaged cells per sample yielded the biovolume-derived $bSiO_2$ associated with the living diatoms — hereafter referred to

as "live" $bSiO_2$ to distinguish it from total (living plus detrital) $bSiO_2$. While this relationship works well for ASGARD and other Southern Ocean field datasets, it does not appear to be accurate for more temperate cold water systems like in the northern Kerguelen Plateau — discussed in Krause and Lomas (2020). However, this specific allometric relationship has been shown to yield growth rates that are realistic, i.e. 1 – 64% of the maximum predicted growth rate based on the temperature of collection (Eppley, 1972), compared to Si per biovolume relationships derived from low-latitude diatoms in culture and field studies (Conley et al., 1989; Krause et al., 2010), which can yield growth rates ranging from 6 – 294% (average 110%) of that predicted by the temperature (Krause and Lomas, 2020). The underlying mechanisms responsible for the Lomas et al. (2019) allometry success and/or unsuccess in specific cold-water systems requires more study. However, for this analysis, this allometry is favored based on collectively yielding the most realistic growth rates given the ambient temperatures.

2.3. Diatom production and growth rates

For $bSiO_2$ production, measurements were made using a radioisotope (Krause et al., 2011). After gently homogenizing the carboy, triplicate 150 mL polycarbonate bottles were filled at the same time as dilution experiment bottles. To each replicate, 367 Bq of $^{32}Si(OH)_4$ (>20 kBq µg Si^{-1}) was added, bottles were capped and sealed, and placed in bags made of neutral density screening to simulate the $\%I_0$ at the depth of collection. Bags were then submerged in a transparent acrylic deck-board incubator continuously cooled with shipboard water pumped from their underway system intake (~6 m depth, ~50%I_0 depth). Incubations were terminated after 24 hours and samples were filtered onto a 1.2 µm pore polycarbonate filter, dried on Nylon disc planchettes, then covered with mylar that was secured with a nylon ring to keep the filter and particles contained. ^{32}Si (long-lived parent, half-life ~140 years) decays into a short-lived daughter isotope, ^{32}P (half-life ~14 days); samples were stored for ~4 months (i.e. seven ^{32}P half-lives) to reach secular equilibrium and avoid quantification of any activity on the filter which was from the uptake of ^{32}P. Planchette ^{32}Si activity was quantified using gas-flow proportional counting with a GM-25 multicounter (Risø National Laboratory, Technical University of Denmark) as described by (Krause et al., 2011). The gross rate of $bSiO_2$ production is referred to

as ρ (µmol Si L^{-1} d^{-1}), and was normalized to the total standing stock of $bSiO_2$ to determine the biomass-specific rate of production, denoted as V_b, using a logistic approach:

$$bSiO_{2\text{-New}} = \rho \text{ x (incubation time)}$$

$$V_b = \ln[(bSiO_{2\text{-New}} + \text{average } bSiO_2) \text{ x (average } bSiO_2)^{-1}] \text{ x (incubation time)}^{-1}$$

where the average $bSiO_2$ represents the average of the triplicate samples at the same sampling point. Combining the ^{32}Si uptake and live $bSiO_2$ facilitated estimation of diatom growth rates (µ) (Krause and Lomas, 2020) as:

$$\text{diatom } \mu = \rho \text{ x (live } bSiO_2)^{-1}$$

In four (out of 24 total) cases, live $bSiO_2$ exceeded the total $bSiO_2$ from the filtered samples (102, 134, 138, 316%); for these instances, diatom µ was calculated using the filtration-based total $bSiO_2$ assuming that all $bSiO_2$ was living (i.e. V_b and diatom µ are equal). Both V_b and diatom µ enable estimates of doubling times following:

$$\text{doubling time} = (V_b \text{ or diatom } \mu) \text{ x } \ln(2)$$

The comparison of diatom µ and ≥5 µm phytoplankton µ (dilution experiment, see below) is not straight forward, even if diatoms represent 100% of the ≥5 µm Chl *a*, due to these measurements quantifying different aspects of diatom cell growth. The dilution method derives estimates of µ from net changes in cell-associated Chl *a* under variable MZP grazing losses. These changes can be positive or negative and may not necessarily reflect cell division. ^{32}Si-based estimates of diatom µ are based on the rate at which Si is incorporated into diatom frustules (typically occurs immediately prior to division) and normalized to live $bSiO_2$; because of the tracer addition approach, only positive rates are valid. There are known temporal offsets between these two processes within a diatom cell. If the incubation period is less than a cell division cycle, then it would be expected that these measurements of diatom µ and ≥5 µm µ are uncoupled. Given the 24-hour incubation conditions, and that regional diatoms have been shown to grow at a doubling every two days (Yang et al., 2015), these independent growth metrics are not expected to be well aligned for this system even when diatom biomass dominates this size fraction.

2.4. Microzooplankton grazing and phytoplankton growth rates

Microzooplankton grazing and phytoplankton μ were quantified for each Chl *a* size fraction, ≥5 μm and < 5 μm, using a modified dilution experiment assay similar to previous regional studies (Olson and Strom, 2002; Sherr et al., 2013; Stoecker et al., 2014a; Strom and Fredrickson, 2008; Yang et al., 2015). This method has been widely used and reviewed elsewhere (Calbet and Landry, 2004); briefly, it assumes that predictable changes in encounter rate between MZP and phytoplankton prey affect the net accumulation of phytoplankton biomass (e.g. Chl a) proportionally, i.e. reducing the interaction increases the relative net accumulation of Chl *a* due to the easing of grazing pressure. A second Niskin bottle at each light depth was used to generate particle-free seawater (i.e. exclusion of bacteria and microplankton). Water was directly subsampled from the Niskin bottle through 0.2 μm capsule filter (with a built-in 0.8 μm pre-filter), using a peristaltic pump, into 1-L incubation bottles in four proportions (based on the dilution percentage); these ranged from 100% whole seawater to 15% whole seawater (i.e. 85% particle-free seawater). For each experiment (i.e. depth and station), four dilution levels were used, and every level had triplicate bottles. After gently homogenizing water from the 200 μm-prefiltered carboy, whole seawater was added to the particle-free seawater in each dilution bottle, slowly (with minimal turbulence) bringing all 1 L bottles to a constant volume (i.e. the bottle brim), and sealing the bottle opening with laboratory parafilm to avoid any air bubbles after the bottle cap was placed (M. Landry, pers. comm.). A nutrient amendment was made (5 μM nitrate, 0.5 μM phosphate) when nitrate concentrations in the water were <1 μM based on shipboard underway In Situ Ultraviolet Spectrophotometer sensor to avoid exacerbating potential nutrient limitation by lack of MZP-based nutrient remineralization in highly diluted samples. Post cruise nutrient data showed inconsistencies between the underway nitrate estimate and that from the direct nutrient analysis, specifically that some nutrients were low when the sensor measurement reported high values. Many studies use unamended 100% whole seawater controls to compare with nutrient-amendment bottles, e.g. (Olson and Strom, 2002; Yang et al., 2015); however, similar to Sherr et al. (2013), who were also involved in a large and multidisciplinary cruise, we did not have the water budget to include unamended controls, as these would have resulted in no volume for diatom production measurements (above). Regional studies, during summer, show that the growth rate for non-amended controls are typically 80% – 100% of rates in the amended controls among phytoplankton groups (Yang et al., 2015). Sample bottles (12 per depth) were placed in corresponding neutral density screened bags and incubated alongside ^{32}Si samples.

285 Initial Chl *a* samples were immediately filtered following placement of samples in the incubator
286 and final Chl *a* samples were filtered after the 24-hour incubation; both were size-fractionated
287 and quantified at sea as described above. The initial Chl *a* was averaged among triplicates and
288 multiplied by each dilution factor to obtain the initial Chl *a* concentration for each dilution. Flow
289 cytometry subsamples (2 mL) were collected from all Chl *a* sample bottles prior to filtration.
290 These samples were preserved (0.5% paraformaldehyde final concentration), frozen at -80 °C,
291 analyzed as described elsewhere (Casey et al., 2013), and were used to quantify potential
292 photoacclimation effects during the incubation. During analysis, the relative red fluorescence of
293 phytoplankton particles was compared to a standard reference bead (Spherotech; 0.53 µm Nile
294 Red), which was checked and adjusted (if necessary) every half hour while samples were being
295 analyzed to ensure consistency of instrument performance through the analytical run. When the
296 ratio of red fluorescence in the final samples to the initial samples (PA_{corr}) exceeded 1.0, we
297 interpreted that photoacclimation occurred and used this to empirically correct calculated rates
298 (discussed below).
299 Net changes in Chl *a* as a function of dilution were used to determine the parameters of
300 interest. Particle-free seawater blanks typically had barely detectable or below-detection Chl *a.*
301 For every individual replicate among dilution levels, the net rate of Chl *a* change was calculated
302 as:
303 $$\text{Net Chl } a \text{ rate} = \ln(\text{Chl } a \text{ final} \times \text{Chl } a \text{ initial}^{-1} \times PA_{corr}^{-1}) \times \text{incubation time}^{-1}$$
304 thus, 12 points were generated among the four dilution levels for each size fraction.
305 Operationally, PA_{corr} values for picoeukaryotes and nanoeukaryotes were assigned for the <5 and
306 ≥5 µm fractions, respectively. The increased temperature of incubation relative to that at the
307 collection of sampling may have artificially increased phytoplankton growth rates. Among the 15
308 stations, the temperature at the $50\%I_0$ during collection was 0 – 5.9 °C higher than the lower-
309 light sample depth, with the median and average being 2.1°C and 2.2 °C, respectively. Given the
310 lower light conditions which persisted throughout the incubation, we presume that light was the
311 most salient limiting factor (see Discussion) and chose not to apply any temperature corrections
312 in this analysis. A Model I linear regression was fit to each data set (i.e. <5, ≥5 µm size fractions)
313 where the slope denotes the specific MZP grazing rate (denoted as g, d^{-1}) and the y-intercept the
314 instantaneous phytoplankton growth rate (denoted as µ, d^{-1}, i.e. the rate of growth when no MZP
315 grazers are present). For these regression fits, an $\alpha = 0.05$ level was used to denote the

316 probability of rejecting the null hypotheses (i.e. MZP grazing and phytoplankton growth rates
317 were zero) when true. Under conditions when we could not reject the null hypothesis for a
318 specific rate (i.e. grazing, growth), we considered it below detection for that experiment and a
319 value of zero was assigned for purposes of averaging rates among stations. The proportion of
320 phytoplankton growth consumed by MZP grazing was estimated as: $g \times \mu^{-1}$ for each size
321 fraction, depth, and station. To distinguish dilution-experiment derived μ from diatom growth
322 rate derived using ^{32}Si (above), dilution-based growth rates will be referred to with their
323 corresponding size fraction (e.g. <5 μm μ and ≥5 μm μ).
324
325 *2.5. Historical data and statistical analysis*
326
327 To contextualize our results, MZP grazing rate data from previous studies were compiled
328 from published tables (Liu et al., 2002; Olson and Strom, 2002; Sherr et al., 2009; Sherr et al.,
329 2013; Strom and Fredrickson, 2008; Yang et al., 2015). For data only reported in figures
330 (Connell et al., 2018; Olson and Strom, 2002), Graph Grabber (Quintessa software) was used to
331 extract these data. In other studies (Stoecker et al., 2014a), data were available in public archives.
332 Because we could not directly compare our size fractionated rates with these previous studies
333 (for which size fractionation may not have been conducted), rates were compared based on total
334 Chl *a* (i.e. sum of our size fractions).
335 Statistics were run using XLStat software. For correlation analyses, a non-parametric
336 Spearman Rho test was used, and comparison between sample types was also done using a non-
337 parametric Mann Whitney U test. For model II regressions, a geometric mean regression
338 approach was used. To determine factors that affected diatom growth rates, an ANCOVA
339 approach was used to generate a best fit model determined using the Akaike Information
340 Criterion (AIC). The goal of this model was to assess the relative importance of measured
341 properties (e.g. nutrient concentrations), categorical variables (e.g. high and low light), and/or
342 their interaction, in explaining variance among diatom growth rates.
343
344 **3. Results**
345
346 *3.1. Hydrography and nutrients*

347

348 The general climatology during ASGARD 2017 was warm relative to average conditions
349 (Danielson et al., 2020; Huntington et al., 2020). Generally, the progression of sea-ice retreat was
350 consistent from south to north based on data within three subareas in the southeastern BS,
351 northern BS, and the CS (Fig. 1). An oscillation between warm and cold intervals between 2000
352 – 2019 for a small area in the southeastern BS (Fig. 1B) alters the ice retreat timing by plus or
353 minus one month compared to mean conditions (Stabeno et al., 2012), though recent conditions
354 have shown more dramatic changes (Baker et al., 2020; Huntington et al., 2020; Walsh et al.,
355 2018). Fractional ice cover in the southeastern and northern BS during June 2017 (Fig. 1D) were
356 consistent with previous decades for this time of the year (i.e. low), yet the ice extent in the
357 northern BS appeared to be declining in April and May relative to the long-term record. During
358 June, the average ice cover (mean ± SD used throughout Results unless otherwise noted) in the
359 northern BS was 3.4% ± 2.7% from 1980 through 2006, but from 2007 through 2017 it was 0.4%
360 ± 0.5%. Relative to the years 1980 through 2019, the extent of ice-free water in the CS during
361 June 2017 was highest during this time series (Fig. 1D) and with only minimal changes in the
362 following two years after the cruise (June 2018, June 2019). This reduction trajectory appears to
363 be a long-term, albeit highly variable, trend since 1980 (Fig. 1D). Within the water column, we
364 consistently observed thermal stratification (as expected). Among our incubation stations, the
365 upper euphotic zone samples (3 – 7 m) came from waters ranging between 2.4 – 6.5 °C, while
366 for the lower euphotic zone samples (10 – 35 m) the water temperature at the time of sampling
367 ranged between -1.2 – 4.0 °C (Table 1, Fig. 2).

368 Nutrient concentrations were variable laterally across the shelf, but increased with depth
369 (Table 1, Fig. 2). In the upper euphotic zone, the ranges (mean ± SD) for phosphate, nitrate,
370 ammonium, and silicic acid were 0.3 – 1.7 µM (0.7 ± 0.4 µM), 0.0 – 16.7 µM (3.1 ± 5.9 µM),
371 0.0 – 1.5 µM (0.4 ± 0.5 µM), 0.5 – 31.4 µM (6.7 ± 10.1 µM), respectively. In the lower euphotic
372 zone, the ranges (mean ± SD) for phosphate, nitrate, ammonium, and silicic acid were 0.6 – 1.8
373 µM (1.0 ± 0.4 µM), 0.0 – 17.9 µM (5.0 ± 6.7 µM), 0.0 – 4.4 µM (1.3 ± 1.0 µM), 0.7 – 33.4 µM
374 (9.5 ± 11.1 µM), respectively. Most of the variability in both diatom V_b and diatom µ was
375 accounted for by variability in nitrate and silicic acid concentrations (discussed below); thus,
376 phosphate and ammonium are not discussed further. The heterogeneity across the nutrient fields
377 reflects a combination of unresolved lateral variations in the flow and water mass fields, time

history of each water parcel in relation to the spring bloom, and the energetic local flow field adjusting to the topographic constrictions of the Bering Strait region (Danielson et al., 2020; Danielson et al., 2014).

3.2. Phytoplankton community and diatom biomass

As with nutrients, Chl *a* concentrations were highly variable station-to-station (Table 1, Fig. 2). Among the 28 sample depths, five were considered to be at bloom biomass (>3.0 µg Chl *a* L^{-1}, Table 1), based on the regional criterion reported in Sherr et al. (2013). For upper euphotic zone samples, ≥5 µm Chl *a* ranged from <0.1 – 16.5 µg L^{-1} with an average of 1.7 ± 4.4 µg L^{-1} (Fig. 2C), while <5 µm Chl *a* ranged from <0.1 – 0.8 µg L^{-1} with an average of 0.3 ± 0.3 µg L^{-1} Replication for Chl *a* in both size fractions was acceptable, with the average (± SD) percent coefficient of variation (CV) being 14 ± 9% and 21 ± 15% for the large and small size fractions, respectively. Lower euphotic zone samples were similar in range to upper euphotic zone samples; 0.2 – 17.6 µg L^{-1} for ≥5 µm Chl *a* and <0.1 – 0.8 µg L^{-1} for <5 µm Chl *a*; with average values of 2.5 ± 4.6 µg L^{-1} and 0.3 ± 0.2 µg L^{-1} for the ≥5 µm and <5 µm Chl *a* fractions, respectively. For these lower euphotic zone samples, the average percent CV was 22 ± 22% and 25 ± 20% for the large and small size fractions, respectively. When averaging among all stations and depths, the ≥5 µm fraction had the majority of Chl *a,* and this increased from the upper euphotic zone (55 ± 28%) to the lower euphotic zone (75 ± 21%).

Like ≥5 µm Chl *a*, $bSiO_2$ (i.e. diatom biomass proxy) had a similar degree of station-to-station variability (Fig. 2D, 2I). In the upper euphotic zone, $bSiO_2$ ranged from 0.5 – 14.5 µmol Si L^{-1} (Fig. 2D) with an average (± SD) of 4.5 ± 4.8 µmol Si L^{-1}. In the lower euphotic zone, $bSiO_2$ ranged from 1.9 – 15.2 µmol Si L^{-1} (Fig. 2I) with a significantly higher average, 8.2 ± 4.4 µmol Si L^{-1}, than the upper euphotic zone (Mann-Whitney U = 53, $p<0.05$; Fig. 2D, 2I). The CV among total $bSiO_2$ replicates was better than for both Chl *a* size fractions, averaging 9 ± 15% and 6 ± 5% for upper and lower euphotic zone, respectively. The percentage of live $bSiO_2$, which was associated with living diatoms (Table 1), ranged from 4 – 316% (average 60% ± 90%) and 2 – 190% (average 38% ± 56%) for the upper and lower euphotic zones, respectively. As noted above in the Methods section, only four samples exceeded 100% (Table 1), and when assigning 100% to these depths, the averages (± SD) were reduced to 37 ± 38% and 30 ± 34% for the upper

409 and lower euphotic zone, respectively. Correlations between total and live $bSiO_2$ with ≥5 µm Chl
410 *a* were strong and all highly significant: ≥5 µm Chl *a* vs. total $bSiO_2$ (Spearman Rho = 0.87,
411 $p<0.01$), ≥5 µm Chl *a* vs. live $bSiO_2$ (Spearman Rho = 0.79, $p<0.01$). These results suggest that
412 diatoms were the dominant phytoplankton group modulating the signal in the larger Chl *a* size
413 fraction.
414
415 *3.3. Diatom $bSiO_2$ production and growth rates*
416 Diatom $bSiO_2$ production generally mirrored the trends in biomass (Table 1, 2). The
417 gross rate of $bSiO_2$ production, ρ, was highly correlated with total $bSiO_2$ standing stock
418 (Spearman Rho = 0.75, $p<0.01$) and ≥5 µm Chl *a* (Spearman Rho = 0.85, $p<0.01$). ρ ranged from
419 0.01 – 1.81 µmol Si L^{-1} d^{-1} (average 0.35 ± 0.59 µmol Si L^{-1} d^{-1}) and <0.01 – 2.03 µmol Si L^{-1} d^{-1}
420 (average 0.38 ± 0.64 µmol Si L^{-1} d^{-1}) for the upper and lower euphotic zones, respectively. Like
421 other replicated measurements, the CV was low, with averages of 12 ± 7% and 12 ± 6% for the
422 upper and lower euphotic zones, respectively. V_b ranged from 0.01 – 0.17 d^{-1} and <0.01 – 0.14 d^{-1}
423 for the upper and lower euphotic zone, respectively; the averages (± SD) at each light depth
424 were also similar (upper euphotic zone 0.05 ± 0.05 d^{-1}, lower euphotic zone 0.03 ± 0.04 d^{-1}).
425 Maximum V_b (i.e. 0.17 d^{-1}) infers a minimum doubling time of 4.1 days; however, the doubling
426 time averaged (± SD) station-by-station (opposed to basing on average V_b) inferred was 34 ± 24
427 and 82 ± 86 days for the upper and lower euphotic zone, respectively.
428 Diatom µ can help correct for potential bias of V_b rates due to detrital $bSiO_2$. V_b and
429 diatom µ among stations and depths were not significantly correlated (Spearman Rho = 0.07,
430 $p=0.73$), which is expected if there was a variable proportion of detrital $bSiO_2$ among stations
431 (Goering et al., 1973; Krause et al., 2010). Diatom µ exceeded V_b in all but four samples (i.e.
432 those where live $bSiO_2$ was >100%). Diatom µ ranged from 0.02 – 0.68 d^{-1} (average 0.20 ± 0.19
433 d^{-1}) and 0.05 – 0.79 d^{-1} (0.17 ± 0.21 d^{-1}) in the upper and lower euphotic zone, respectively. The
434 station-by-station average doubling times averaged (± SD) 9 ± 11and 7 ± 4 days for the upper
435 and lower euphotic zone, respectively. We infer that diatom µ estimates are reflective of
436 phytoplankton in only the large size fraction (discussed below); this is bolstered by the strong
437 correlations between ≥5 µm Chl *a* and live $bSiO_2$ (see above), ≥5 µm Chl *a* and ρ (see above),
438 and no correlation between <5 µm Chl *a* and either live $bSiO_2$ (Spearman Rho = 0.00, $p=0.97$) or
439 ρ (Spearman Rho = 0.03, $p=0.89$).

Using an ANCOVA approach, a statistical model was produced to identify and quantify the degree of diatom μ variability explained by nutrients, light, and their interaction. Using AIC, the best fit models using 1, 2 and 3 parameters were generated. Given that we sampled at relative light depths (i.e. 50%I_0 and 5%I_0 or 1%I_0) for a given experiment, light was used as a categorical variable, i.e. high (n = 13) or low (n = 10) in the ANCOVA. A one interaction model (nitrate x light) explained a majority of the variance (model $F_{(1, 21)} = 40.9$, $p<0.01$, $r^2 = 0.66$, AIC = -107.9; Supplementary Table 1, 2). The two- and three-variable models selected could explain a higher proportion of diatom μ variance but only with a minor change in AIC (e.g. two variable: light, silicic acid x light $r^2 = 0.72$, ΔAIC 2.4; three variable: ammonium, light, silicic acid x light $r^2 = 0.77$, ΔAIC 4.6; Supplementary Table 1, 2).

3.4. Size-fractionated phytoplankton community rates: MZP grazing loss and phytoplankton growth

Whether MZP grazing rates were quantifiable experimentally was strongly dependent on the phytoplankton size class (Fig. 3). Among the 28 experiments (i.e. 14 stations, 2 depths per station), significant grazing for the ≥5 μm Chl *a* size fraction was observed in 10 experiments (Table 2); the lack of quantifiable grazing did not appear to result from the absence of nutrient amendments, as five experiments (of the 10 with quantifiable grazing) had amended nutrients and five did not. This differs from the <5 μm Chl *a* size fraction, where significant grazing was observed in 21 of 27 experiments (Table 2; <5 μm Chl *a* initial samples were compromised for one experiment/depth hence the lower total number of experiments). For the ≥5 μm Chl *a* size fraction, grazing rates ranged from 0 – 3.33 d^{-1} (average 0.35 ± 0.89 d^{-1}) in the upper euphotic zone and 0 – 2.95 d^{-1} (average 0.31 ± 0.78 d^{-1}) in the lower euphotic zone (Table 2). Among these same stations and depths, the growth rate for the ≥5 μm Chl *a* size fraction ranged from -0.50 – 1.40 d^{-1} (average 0.09 ± 0.43 d^{-1}) and -0.10 – 1.00 d^{-1} (average 0.09 ± 0.27 d^{-1}) in the upper and lower euphotic zones, respectively. In the <5 μm Chl *a* size fraction, grazing rates ranged from 0 – 2.71 d^{-1} (average 0.62 ± 0.77 d^{-1}) in the upper euphotic zone and 0 – 2.30 d^{-1} (average 0.57 ± 0.57 d^{-1}) in the lower euphotic zone (Table 2). The corresponding range in growth rates for the <5 μm Chl *a* size fraction ranged from 0 – 2.00 d^{-1} (average 0.48 ± 0.54 d^{-1})

and -0.42 – 1.77 d^{-1} (average 0.50 ± 0.54 d^{-1}) in the upper and lower euphotic zones, respectively.

MZP grazing rates were significant at times relative to phytoplankton growth rates. When comparing MZP g to phytoplankton μ, Sherr et al. (2013) included all stations, regardless of whether or not MZP grazing was significantly resolved; for consistency, we report g μ^{-1} for both size fractions in this manner (Table 2). However, for our calculations of averages, we considered 0 values for grazing when MZP was not significant. For the ≥5 μm Chl *a* size fraction the percentage of grazing relative to growth ranged from 0 – 314% (average 47% ± 100%) and 0 – 295% (average 51% ± 91%) in the upper and lower euphotic zones, respectively. For the <5 μm Chl *a* size fraction the percentage of grazing relative to growth ranged from 0 – 197% (average 87% ± 64%) and 0 – 147% (average 97% ± 37%) in the upper and lower euphotic zones, respectively. As reported by Sherr et al. (2013), we also observed a major shift in g μ^{-1} between bloom and non-bloom stations, but only for the large size fraction. Average (± SD) ≥5 μm g μ^{-1} was 23% ± 35% (55% ± 102%) for bloom (non-bloom) stations. Whereas average <5 μm g μ^{-1} was 64% ± 38% (79% ± 63%) for bloom (non-bloom) stations.

4. Discussion

4.1. Bottom-up regulation of phytoplankton growth rates

Dilution experiments enable an assessment of both bottom-up and top-down factors concurrently. The caveat for comparing phytoplankton growth rates to bottom-up factors is that dilution experiments must successfully conform to the methodological assumptions (Landry and Hassett, 1982). Non-zero rates for the small-phytoplankton size class were quantified in 70% of our experiments, twice the number of experiments where non-zero rates were quantified for large phytoplankton. A correlation analysis among all hydrographic (temperature, water depth), chemical (nitrate, ammonium, phosphate, silicic acid) and particulate (size fractionated Chl a, total $bSiO_2$, live $bSiO_2$) stocks, and process rates (<5 μm and ≥5 μm μ, MZP grazing on both size fractions, diatom μ, ρ, V_b) showed that the growth rate for small phytoplankton was significantly correlated with only the growth rate of large phytoplankton and the MZP grazing

rate of small phytoplankton (Spearman Rho = 0.72, $p<0.01$). These correlations suggest MZP controlled <5 µm µ but not biomass in this size fraction. This lack of correlation may be an artifact of the relatively invariant <5 µm biomass (Chl *a* range <0.1 – 1.1 µg L^{-1}, average 0.3 ± 0.2 µg L^{-1}) and lower dynamic range than biomass in large cells, hence a correlation could not resolve a biomass trend. Additionally, the lack of correlation to hydrographic parameters and nutrients could reflect the tight coupling between small phytoplankton growth and MZP grazing at both light depths (i.e. MZP grazed, on average, 87% ± 64% and 97% ± 37% of production for upper and lower euphotic zone, respectively), suggesting that food web/ecological processes (nutrient remineralization) were more important for sustaining <5 µm µ during our cruise.

Given the consistency in observed growth and MZP loss rates for small phytoplankton, the remainder of the discussion focuses on processes in the large phytoplankton size fractions, specifically for diatoms. Quantifiable non-zero growth rates in the large phytoplankton occurred in 35% of the experiments. The tight coupling between ≥5 µm Chl *a* and total $bSiO_2$, live $bSiO_2$, and ρ strongly support the notion that diatoms drove the signal in the large phytoplankton size fraction, consistent with previous regional studies (Baumann et al., 2014; Giesbrecht and Varela, 2021). We leverage the independent isotope-based diatom growth rates in the remaining analyses due to the high frequency of zero rates quantified for dilution experiments (discussed below).

There are few previous studies reporting ρ, V_b or diatom µ data in this region. During the Processes and Resources of the Bering Sea Shelf program from 1978 – 1981, Banahan and Goering (1986) reported ρ or V_b in the southeastern Bering Shelf region, the same spatial domain as more recent projects (e.g. BEST). Their sampling included higher vertical resolution, but euphotic zone average ρ (i.e. their reported integrated rate divided by euphotic zone depth) ranged from <0.1 – 1.1 µmol Si L^{-1} d^{-1}, with their highest single-depth rates exceeding 2 µmol Si L^{-1} d^{-1}; these ranges are nearly identical to our observations. Similarly, their range in euphotic-zone averaged V_b was 0.04 – 0.18 d^{-1}, similar to our rates during the ASGARD cruise (note: these authors normalized to total particulate silica opposed to just $bSiO_2$, suggesting rates were conservative). More recently, Giesbrecht and Varela (2021) reported the first measurements for ρ or V_b within the euphotic zone of the ASGARD domain (i.e. northern BS and CS) during July with multiple years of data (2013 – 2016). Giesbrecht and Varela (2021) observed higher maximum ρ and V_b values, with rates up to >3 µmol Si L^{-1} d^{-1} and >0.3 d^{-1}, respectively; however, the time-averaged ρ among all stations and summers was <0.5 µmol Si L^{-1} d^{-1} except

for a single station in the Bering Strait (average ~2 µmol Si L^{-1} d^{-1}) which was more variable. Similarly, the central tendency for average V_b among years and stations reported by Giesbrecht and Varela (2021) was <0.2 d^{-1} for all stations except the Bering Strait (~0.3 d^{-1}). Yang et al. (2015) also used a dilution method approach in the CS (73° – 79° N) during summer under primarily low Chl *a* conditions (<0.6 µg L^{-1}); however, these authors used diatom cell counts to quantify growth, making a better comparison to our isotope-derived diatom µ (shown in Fig. 4D). These authors reported a range of 0.16 – 0.45 d^{-1}, with an average of 0.30 ± 0.10 d^{-1}. Overall, rates during ASGARD appear comparable to previous studies (in both spring and summer) despite the anomalously low ice conditions during June 2017 (Fig. 1D).

The comparison of V_b vs. silicic acid concentration can yield important information about whether diatoms may be kinetically limited by silicic acid availability. While kinetic limitation may not be intense enough to dramatically limit diatom growth, even moderate stress (e.g. uptake of Si at half saturation rates) has been linked to increased mortality through facilitation of viral infection both in laboratory conditions and the California Current during upwelling (Kranzler et al., 2019). A saturable response (e.g. Michaelis-Menten kinetics) is expected when examining V_b vs. silicic acid concentration, yet such a trend is only apparent for a subset of our data (Fig. 4A). Saturable responses are observed when a single community (i.e. specific station and water depth) is amended with increasing silicic acid to observe the response of Si uptake, e.g. Giesbrecht and Varela (2021) during summer, whereas we report uptake rates among different communities across a natural gradient in silicic acid. Consequently, each community likely has a different physiological acclimation state, sensu Lomas et al. (2014), which complicates using a Michaelis-Menten kinetic framework to infer limitation of diatoms by suboptimal silicic acid concentrations (hence using ANCOVA approach, discussed below). Low V_b values are associated with both high and low silicic acid concentrations (Fig. 4A). We infer this to be due to low diatom activity (e.g. early bloom phases, high nutrients) and/or an artefact of high detrital silica which biases V_b to be low (e.g. late bloom phase, low nutrients). The subset of samples that appear to have a Michaelis-Menten response (i.e. all V_b > 0.03 d^{-1}, except the DBO2.2, 4m sample) only share the commonality of high live $bSiO_2$ percentage (73 ± 30%) vs. all other samples (18 ± 24%, Fig. 4A) and these differences are significant (Mann-Whitney U = 24, p=0.01). Correcting for effects of detrital $bSiO_2$ shows that diatom µ was well correlated to bottom-up factors (Fig. 4B, 4C). The relatively linear response, opposed to a hyperbolic response

observed in short-term experiments, e.g. Giesbrecht and Varela (2021), observed between diatom μ and nutrients (Fig. 4B, 4C) is consistent with acclimation to the mean environment, as alluded to for P by Lomas et al. (2014). Taken together, this suggests that silicic acid concentration did not limit diatom growth during ASGARD.

Our data suggest that diatom μ may have been lower than physiological maxima. Using Eppley's classical empirical equation showing the change in phytoplankton growth with temperature (Eppley, 1972), upper euphotic zone diatoms grew at an average of 20 ± 19% of their maximum rate, and lower euphotic zone diatoms grew at an average of 18 ± 24% of their maximum rate (Fig. 4D). Given the similarity of diatom rates to previous regional reports, it may be inferred that growth could have been limited in those studies also. Due to the high degree of correlation between silicic acid and nitrate concentrations (Spearman Rho = 0.94, $p<0.01$), diatom μ increased linearly in response to increases of both nutrients (Fig. 4B, 4C), thereby making it difficult to assign one as the limiting nutrient over the other; however, the ANCOVA results show that the interaction of nitrate and light provides the most predictive power for a one-parameter model. The rate of increase in diatom μ with increasing nutrient concentrations was also larger for the upper euphotic zone than lower euphotic zone. This separation by light depth suggests an important role for light and/or the interaction of light and nutrients in regulating diatom μ, as observed for lower latitude diatoms (Brzezinski et al., 2015; King and Barbeau, 2011). Even if the effect of light-nutrient interaction has a small absolute magnitude (compared to lower latitude systems), it could be proportionally more important in polar regions due to the relatively low growth rates constrained by ambient temperature. Given the result of the ANCOVA model fit to these data, i.e. the interaction of light and nitrate was the most important factor (explaining 66% of the data set variance), future regional work should explore diatom growth within the context of co-limitation.

4.2. Do MZP control diatoms during spring?

Many ecological interactions among zooplankton and phytoplankton are size-dependent. As phytoplankton increase in size, e.g. large diatoms and/or long chains, they typically become too large for consumption by most MZP and are more favorable for LMZP (e.g. large calanoid copepods, krill), although studies do show BS LMZP prefer MZP (Campbell et al., 2016).

However, many MZP (e.g. certain dinoflagellates) have evolved mechanisms to handle large particles at a fast rate in lower latitudes, especially diatom chains - which may be many times longer than their own body length (Jacobson and Anderson, 1986). While there have been many studies in the region, especially in the southeastern BS, reporting dilution experiment data, most experiments were not size-fractionated and those that did were largely conducted during the summer (Olson and Strom, 2002; Strom and Fredrickson, 2008). When considering the proxy of total Chl *a* (i.e. sum of ≥5 and <5 µm Chl *a* fractions) during spring data from previous studies, the proportion of experiments with no significant MZP grazing (i.e. grazing = 0) was similar to our study (Fig. 5). However, when size-fractionating, the proportion of experiments with MZP grazing rates equal to zero diverged with plankton size, a trend not observed during summer studies (Fig. 5). Given the similarity in our data and prior regional work (when using total Chl *a* as a proxy), we suggest that diatoms during spring largely escape MZP grazing losses, especially during blooms, and we explore explanations for this apparent lack of grazing control.

While large cells may be palatable for MZP, they do present issues of increased handling time and mechanical barriers. Two laboratory studies have demonstrated that MZP prefer diatoms with lower silica content vs. more silica-dense cells (Spillane, 2016; Zhang et al., 2017). Among all samples, only three (5 m DBO3.3, 4 m CPL6, 22 m IL4; Table 1) were dominated numerically by pennate diatoms (e.g. *Fragilariopsis*, *Pseudo-nitzschia*; data not shown), yet only one of these three samples (5 m DBO3.3, Table 2) had significant grazing on large phytoplankton by MZP. Strom et al. (2017) also recently reported there is no evidence that coccolithophorid calcium carbonate plates protect large phytoplankton from MZP grazing. Coccolithophore cells are considerably smaller than diatoms, thus, the combined effect of phytoplankton size and biomineral content may reduce, but not eliminate MZP grazing rates, e.g. (Jacobson and Anderson, 1986). In the Bering and Chukchi environments, this size-selectivity of MZP for smaller phytoplankton may manifest if the large phytoplankton assemblage is dominated by heavily silicified chain-forming centric diatoms as opposed to lightly silicified chain-forming pennate diatoms (Taniguchi et al., 1976). During spring 2017, we observed diatom assemblages most of the time were dominated by centric diatoms. Thus, it does not appear that diatom diversity or biomineralization directly promoted escape from MZP grazing.

Top-down control on MZP by LMZP could promote MZP grazing release from diatoms. Regional LMZP appear to prefer MZP, over diatoms, in their diets (Campbell et al., 2016).

However, Campbell et al. (2016) also noted that diatoms were the main diet of LMZP at bloom stations during spring in the eastern BS due to the exceptional disparity between diatom biomass and MZP biomass (i.e. LMZP cannot avoid eating diatoms in bloom conditions). During the ASGARD cruise, LMZP abundances were highly variable among stations and typically dominated by copepods (Kimura et al., 2020). None of the stations sampled by Kimura et al. (2020) were at our bloom stations (CNL3, DBO3.8A, DBO3.8, Table 1). The greatest LMZP abundances for the 2017 growing season (June – September) were observed in the month following the ASGARD cruise for the majority of LMZP species reported (Kimura et al., 2020). While top-down control on MZP cannot be directly tested with these data, we suggest that this was not a main mechanism based on the high spatial and temporal variability reported by Kimura et al. (2020) and the observations by Campbell et al. (2016) that LMZP primarily consume diatoms (despite preferring MZP) under bloom conditions.

The lack of significant grazing on the diatom size class by MZP may be a function of the time lags between these groups. During early bloom stages in this region, MZP growth rates are lower than diatoms due to the lower availability of phytoplankton prey; thus, the conditions of low MZP grazing losses for diatoms encountered during ASGARD may be due to this temporal disconnect (Sherr et al., 2013). Sherr and Sherr (2007) noted that heterotrophic dinoflagellates in the CS and Beaufort Sea are likely dominant consumers of diatom blooms during spring, consistent with other subarctic literature in the northern hemisphere (references therein). However, their analysis was largely based on comparison of standing stocks, without corresponding rate information for all data points. At the three stations with the highest proportion of grazing on large phytoplankton by MZP (CNL3, 4 m; DBO3.3, 5 m; CL3, 22 m; Table 2), FlowCam analysis (data not shown) showed that ciliates dominated MZP biovolume in two (CNL3, DBO3.3) whereas large dinoflagellates (presumably heterotrophic) dominated only at CL3. Overall, the FlowCam-derived MZP biomass (based on allometry) was relatively low (average ~20 µg C L^{-1}, 1st – 3rd quartiles 6 – 30 µg C L^{-1}; Lomas, Krause, unpubl.), especially compared to ~100 µg C L^{-1} estimated phytoplankton carbon —inferred by converting average ≥5 µm Chl *a* (average 2.2 ± 4.4 µg L^{-1}) to carbon using a regional Carbon:Chl *a* ratio of ~50 from Lomas et al. (2012). This range is similar to the average MZP standing stocks observed in the BS during spring at phytoplankton bloom (average 42 ± 22 µg C L^{-1}) and non-bloom (average 9.2 ± 7.8 µg C L^{-1}) stations where dilution experiments were conducted (Sherr et al., 2013). Hence, the

disparity between MZP grazing and diatom growth rates during early bloom stages observed during ASGARD appears to be due to the lag of MZP growth rate to availability of phytoplankton prey (i.e. MZP growth approaches maximum rates at high prey biomass levels). While diatom MZP grazing losses during summer in this region have been reported to be the lowest among the various phytoplankton groups (Yang et al., 2015), these data suggest that diatoms during the spring can grow (at times) with minor and/or insignificant losses due to MZP grazing in spring. This is consistent with the low proportional grazing on larger phytoplankton (i.e. ≥5 µm g μ^{-1}) between bloom (average 23% ± 35%) and non-bloom (average 55% ± 102%) stations. Even if including non-significant ≥5 µm g μ^{-1} station data, i.e. as done by Sherr et al. (2013), the ≥5 µm g μ^{-1} during bloom stations would increase (average 43% ± 46%, Fig. 6) and is nearly identical to bloom station g μ^{-1} reported by Sherr et al. (2013) in the spring (average 42% ± 42%). Thus, under bloom conditions, much of the diatom carbon may be available for higher trophic level organisms and/or export.

4.3. The fate of diatom organic matter during spring

Despite diatoms typically being the largest cells among the phytoplankton community, their losses to MZP grazing consumption can be high in many oceanic regions. In the Southern Ocean from the Polar Front and southward, Selph et al. (2001) reported that MZP grazing rate on diatoms was 63% of diatom growth, indicating that a majority of diatom organic matter production was funneled through this MZP food-web pathway; this proportion is comparable to reported diatom losses to MZP during summer in the CS (Yang et al., 2015). Previous studies in the southeastern BS during summer show that MZP grazing on the largest phytoplankton size class (dominated by diatoms) either can consume ~50% (Strom and Fredrickson, 2008) or nearly 100% (Olson and Strom, 2002) of its production. These summer-season results are consistent with global trends (Calbet and Landry, 2004) in the proportional losses of phytoplankton production to MZP grazing. However, our data support the observation and ideas expressed in Sherr et al. (2013), and discussed above, in that diatoms during this spring period can have pulsed periods of growth without major MZP grazing during bloom development, potentially funneling considerable carbon to higher trophic levels and/or export.

The historical context of ice extent within the ASGARD latitude domain shows that 2017 was a low-ice-extent anomaly (Fig. 1), however, this low-ice anomaly trend appeared to start

687 earlier in the southeastern BS (Fig. 1) around 2014, coincident with other observations of
688 extreme level of oceanic heat in Alaskan waters and the North Pacific more generally (Bond et
689 al., 2015; Danielson et al., 2020; Walsh et al., 2018). Our diatom productivity measurements
690 during 2017 are similar to those of both Banahan and Goering (1986) in the southeastern BS, and
691 within the ASGARD domain by Giesbrecht and Varela (2021) between 2013 and 2016;
692 suggesting that physical changes in the ice extent over time had not manifested in major shifts of
693 diatom production by 2017. This is consistent with inferences from Lomas et al. (2012)
694 regarding the need for at least a factor of two changes in total primary productivity to resolve
695 climate change signals in the BS.

696 The ρ data provide an independent metric of diatom productivity and using recently
697 published Si:C for cold-adapted diatoms (Lomas et al. 2019), we can convert diatom $bSiO_2$
698 production into diatom-based primary production (PP). Because $bSiO_2$ and ≥5 µm Chl *a* were so
699 strongly correlated, we infer that any MZP losses for this size class represents loss of diatoms
700 only; the non MZP-grazed diatom PP sets a conservative metric on the amount of diatom
701 material which can be passed directly to higher pelagic trophic levels or exported to the benthos.
702 We converted this direct loss by MZP to diatom carbon units, and then plotted it against the total
703 diatom PP among bloom and non-bloom stations (Fig. 6). Overall, the 2017 ASGARD data
704 suggest that during bloom conditions, the amount of available diatom PP which escapes MZP
705 grazing is 20-50 times higher than available during non-bloom conditions. This range is nearly
706 double the disparity in absolute diatom PP between bloom and no-bloom conditions (i.e. former
707 is ~12-fold higher), suggesting that the bloom conditions not only favor creation of more organic
708 material, but this material can be more efficiently passed to higher trophic organisms and/or
709 exported for consumption in the benthos.

710 The observation that a majority of spring season diatom PP can be available for pelagic
711 higher trophic level consumers or export to the benthos, even during warm-anomaly years with
712 very little sea ice, suggests that there may be some resilience for Arctic diatoms functioning in a
713 warming world. However, this idea has many caveats. IPCC reports predict significant warming
714 in the Arctic region by the end of the century (IPCC, 2014). A recent analysis by Krause and
715 Lomas (2020) suggested that such warming may reduce the diatom elemental density, which is
716 significantly higher for cold-adapted diatoms vs. low-latitude diatoms (Lomas et al., 2019), and
717 such a reduction in elemental density could converge cold-adapted diatoms with the elemental

718 density in lower latitude diatoms, e.g. Menden-Deuer and Lessard (2000). If such a scenario
719 were to happen, then the quality of diatom carbon per cell could be reduced (i.e. less element per
720 cell), and thereby yield less absolute diatom-based PP (i.e. C) even without declines in diatom
721 abundance. Thus, even if the lack of MZP grazing loss to diatom blooms during ASGARD 2017
722 were reflective of future scenarios in a warming world, potential thermally-driven changes in
723 diatom elemental density may lower the absolute surplus diatom PP available for higher trophic
724 organisms in spring. Additionally, warmer temperatures may stimulate both phytoplankton and
725 MZP growth rates, thus, future MZP assemblages may be able to respond faster to the buildup of
726 phytoplankton biomass, and reduce the inferred temporal lag in our study (and that discussed by
727 Sherr et al. (2013) during spring). The combination of warming (which affects diatom elemental
728 density) and/or increased MZP grazing losses both can reduce the surplus diatom PP in this
729 system and modify the food web. Future efforts must attempt to disentangle these effects to
730 better predict how organic matter will flow to higher trophic levels in these ecologically and
731 economically important, but rapidly changing, regions within the broader Arctic.
732
733
734 **Acknowledgements**
735
736 Funding was provided by the National Science Foundation Office of Polar Programs
737 (OCE-1603605, JWK; OCE-1603460; MWL), logistic and vessel support by the North Pacific
738 Research Board (A91-99a and A91-00a to SLD; NA15NMF4720173 to MWL, subaward to
739 JWK), and vessel support from the Alaska Sikuliaq Program (SLD). We thank the ASGARD
740 cruise (SKQ201708T, SKQ201709S) science party and crew including marine technicians S.
741 Hartz, E. Roth; S. Baer, L. Eisner, D. Wiik, T. Martinson, and D. Harlan for logistical support,
742 and S. Acton and W. Dobbins for laboratory support. The original project data are available at
743 the National Science Foundation Arctic Data Center (doi:10.18739/A2SF2MC1D). This
744 manuscript is a product of the North Pacific Research Board Arctic Integrated Ecosystem
745 Research Program, NPRB publication number ArcticIERP-23.
746
747 **Author Contributions:** JWK and MWL conceived of the study which was enabled by
748 collaboration with SLD. All authors collected samples and provided original data from the

ASGARD cruise (led by SLD). Data analysis was led by JWK and MWL. All authors contributed to the writing the manuscript.

References

Baker, M.R., Farley, E.V., Ladd, C., Danielson, S.L., Stafford, K.M., Huntington, H.P., Dickson, D.M., 2020. Integrated ecosystem research in the Pacific Arctic–understanding ecosystem processes, timing and change. Deep-Sea Res. II 177, 104850.

Banahan, S., Goering, J.J., 1986. The production of biogenic silica and its accumulation on the southeastern Bering Sea shelf. Cont. Shelf Res. 5, 199-213.

Baumann, M.S., Moran, S.B., Lomas, M.W., Kelly, R.P., Bell, D.W., Krause, J.W., 2014. Diatom control of the autotrophic community and particle export in the eastern Bering Sea during the recent cold years (2008–2010). J. Mar. Res. 72, 405-444.

Bond, N.A., Cronin, M.F., Freeland, H., Mantua, N., 2015. Causes and impacts of the 2014 warm anomaly in the NE Pacific. Geophys. Res. Lett. 42, 3414-3420.

Brzezinski, M.A., Krause, J.W., Bundy, R.M., Barbeau, K.A., Franks, P.J.S., Goericke, R., Landry, M.R., Stukel, M.R., 2015. Variable influence of iron stress on siliceous biomass and silica production and silicon and carbon export in a frontal zone within the California Current. J. Geophys. Res-Oceans 120, 4654-4669.

Calbet, A., Landry, M.R., 2004. Phytoplankton growth, microzooplankton grazing, and carbon cycling in marine systems. Limnol. Oceanogr. 49, 51-57.

Campbell, R.G., Ashjian, C.J., Sherr, E.B., Sherr, B.F., Lomas, M.W., Ross, C., Alatalo, P., Gelfman, C., Van Keuren, D., 2016. Mesozooplankton grazing during spring sea-ice conditions in the eastern Bering Sea. Deep-Sea Res. II 134, 157-172.

Casey, J.R., Aucan, J.P., Goldberg, S.R., Lomas, M.W., 2013. Changes in partitioning of carbon amongst photosynthetic pico-and nano-plankton groups in the Sargasso Sea in response to changes in the North Atlantic Oscillation. Deep-Sea Res. II 93, 58-70.

Conley, D.J., Kilham, S.S., Theriot, E., 1989. Differences in silica content between marine and fresh-water diatoms. Limnol. Oceanogr. 34, 205-213.

Connell, P.E., Michel, C., Meisterhans, G., Arrigo, K.R., Caron, D.A., 2018. Phytoplankton and bacterial dynamics on the Chukchi Sea Shelf during the spring-summer transition. Mar. Eco. Prog. Ser. 602, 49-62.

Danielson, S., Ahkinga, O., Ashjian, C., Basyuk, E., Cooper, L., Eisner, L., Farley, E., Iken, K., Grebmeier, J., Juranek, L., 2020. Manifestation and consequences of warming and altered heat fluxes over the Bering and Chukchi Sea continental shelves. Deep-Sea Res. II 177, 104781.

Danielson, S.L., Weingartner, T.J., Hedstrom, K.S., Aagaard, K., Woodgate, R., Curchitser, E., Stabeno, P.J., 2014. Coupled wind-forced controls of the Bering–Chukchi shelf circulation and the Bering Strait throughflow: Ekman transport, continental shelf waves, and variations of the Pacific–Arctic sea surface height gradient. Prog. Oceanogr. 125, 40-61.

Eisner, L., Napp, J., Pinchuk, A., Andrews, A., 2014. Climate-mediated changes in zooplankton community structure for the eastern Bering Sea. Deep-Sea Res. II 109, 157-171.

792 Eppley, R.W., 1972. Temperature and phytoplankton growth in the sea. Fish. B.-NOAA 70,
793 1063-1085.
794 FAO, 2016. The State of the World Fisheries and Aquaculture. Food and Agriculture
795 Organization of the United Nations, Rome.
796 Giesbrecht, K.E., Varela, D.E., 2021. Summertime biogenic silica production and silicon
797 limitation in the Pacific Arctic Region from 2006 to 2016. Global Biogeochem. Cy. 35,
798 e2020GB006629.
799 GMAO, 2008. tavgM_2d_flx_Nx: MERRA 2D IAU Diagnostic, Surface Fluxes, Monthly Mean
800 V5.2.0. Goddard Earth Sciences Data and Information Services Center (GES DISC),
801 Greenbelt, MD, USA.
802 Goering, J.J., Nelson, D.M., Carter, J.A., 1973. Silicic acid uptake by natural populations of
803 marine phytoplankton. Deep-Sea Res. 20, 777-789.
804 Grebmeier, J.M., McRoy, C.P., Feder, H.M., 1988. Pelagic-benthic coupling on the shelf of the
805 northern Bering and Chukchi seas. 1. Food supply source and benthic biomass. Mar. Eco.
806 Prog. Ser. 48, 57-67.
807 Hunt, G.L., Coyle, K.O., Eisner, L.B., Farley, E.V., Heintz, R.A., Mueter, F., Napp, J.M.,
808 Overland, J.E., Ressler, P.H., Salo, S., Stabeno, P.J., 2011. Climate impacts on eastern
809 Bering Sea foodwebs: a synthesis of new data and an assessment of the Oscillating Control
810 Hypothesis. ICES J. Mar. Sci. 68, 1230-1243.
811 Huntington, H.P., Danielson, S.L., Wiese, F.K., Baker, M., Boveng, P., Citta, J.J., De Robertis,
812 A., Dickson, D.M., Farley, E., George, J.C., 2020. Evidence suggests potential
813 transformation of the Pacific Arctic ecosystem is underway. Nat. Clim. Change 10, 342-348.
814 IPCC, 2014. Climat Change 2014: Synehtesis Report., in: Core Writing Team, Pachauri, R.K.,
815 Meyer, L.A. (Eds.), Contribution of Working Groups 1, II, and III to the Fifth Assessment
816 Report of the Intergovernmental Panel on Climate Change. IPCC, Geneva, Switzerland, p.
817 151.
818 Jacobson, D.M., Anderson, D.M., 1986. Thecate heterotrophic dinoflagellates - feeding behavior
819 and mechanisms. J. Phycol. 22, 249-258.
820 Kimmel, D., Lamb, J., Murphy, J., Paquin, M., Rogers, L., Sewall, F., Waters, C., 2019. Leading
821 Zooplankton Indicator for the Southeastern Bering Sea: 2019 Rapid Zooplankton
822 Assessment, in: Siddon, E., Zador, S. (Eds.), Ecosystem Status Report 2019: Eastern Bering
823 Sea, Stock Assessment and Fishery Evaluation Report. North Pacific Fishery Management
824 Council, Anchorage, Alaska, United States, pp. 80-84.
825 Kimura, F., Abe, Y., Matsuno, K., Hopcroft, R.R., Yamaguchi, A., 2020. Seasonal changes in
826 the zooplankton community and population structure in the northern Bering Sea from June to
827 September, 2017. Deep-Sea Res. II 181-182, 104901.
828 King, A.L., Barbeau, K.A., 2011. Dissolved iron and macronutrient distributions in the southern
829 California Current System. J. Geophys. Res-Oceans 116, C03018.
830 Kranzler, C.F., Krause, J.W., Brzezinski, M.A., Edwards, B.R., Biggs, W.P., Maniscalco, M.,
831 McCrow, J.P., Van Mooy, B.A.S., Bidle, K.D., Allen, A.E., Thamatrakoln, K., 2019. Silicon
832 limitation facilitates virus infection and mortality of marine diatoms. Nat. Microbiol. 4, 1790-
833 1797.
834 Krause, J.W., Brzezinski, M.A., Jones, J.L., 2011. Application of low level beta counting of ^{32}Si
835 for the measurement of silica production rates in aquatic environments. Mar. Chem. 127, 40-
836 47.

837 Krause, J.W., Brzezinski, M.A., Landry, M.R., Baines, S.B., Nelson, D.M., Selph, K.E., Taylor,
838 A.G., Twining, B.S., 2010. The effects of biogenic silica detritus, zooplankton grazing, and
839 diatom size structure on silicon cycling in the euphotic zone of the eastern equatorial Pacific.
840 Limnol. Oceanogr. 55, 2608-2622.
841 Krause, J.W., Lomas, M.W., 2020. Understanding Diatoms' Past and Future Biogeochemical
842 Role in High-Latitude Seas. Geophys. Res. Lett. 47, e2019GL085602.
843 Landry, M.R., Hassett, R.P., 1982. Estimating the grazing impact of marine micro-zooplankton.
844 Mar. Biol. 67, 283-288.
845 Liu, H., Suzuki, K., Saino, T., 2002. Phytoplankton growth and microzooplankton grazing in the
846 subarctic Pacific Ocean and the Bering Sea during summer 1999. Deep-Sea Res. I 49, 363-
847 375.
848 Lomas, M.W., Baer, S.E., Acton, S., Krause, J.W., 2019. Pumped up by the Cold: Elemental
849 Quotas and Stoichiometry of Polar Diatoms. Front. Mar. Sci. 6, 286.
850 Lomas, M.W., Bonachela, J.A., Levin, S.A., Martiny, A.C., 2014. Impact of ocean
851 phytoplankton diversity on phosphate uptake. P. Natl. Acad. Sci-USA 111, 17540-17545.
852 Lomas, M.W., Eisner, L.B., Gann, J., Baer, S.E., Mordy, C.W., Stabeno, P.J., 2020. Time-series
853 of direct primary production and phytoplankton biomass in the southeastern Bering Sea:
854 Responses to cold and warm stanzas. Mar. Eco. Prog. Ser. 642, 39-54.
855 Lomas, M.W., Moran, S.B., Casey, J.R., Bell, D.W., Tiahlo, M., Whitefield, J., Kelly, R.P.,
856 Mathis, J.T., Cokelet, E.D., 2012. Spatial and seasonal variability of primary production on
857 the Eastern Bering Sea shelf. Deep-Sea Res. II 65-70, 126-140.
858 Menden-Deuer, S., Lessard, E.J., 2000. Carbon to volume relationships for dinoflagellates,
859 diatoms, and other protist plankton. Limnol. Oceanogr. 45, 569-579.
860 Morales, L.V., Granger, J., Chang, B.X., Prokopenko, M.G., Plessen, B., Gradinger, R., Sigman,
861 D.M., 2014. Elevated 15N/14N in particulate organic matter, zooplankton, and diatom
862 frustule-bound nitrogen in the ice-covered water column of the Bering Sea eastern shelf.
863 Deep-Sea Res. II 109, 100-111.
864 Mordy, C.W., Cokelet, E.D., Ladd, C., Menzia, F.A., Proctor, P., Stabeno, P.J., Wisegarver, E.,
865 2012. Net community production on the middle shelf of the eastern Bering Sea. Deep-Sea
866 Res. II 65-70, 110-125.
867 Nielsen, J.M., Mordy, C.W., Bell, S.W., Lomas, M.W., Stabeno, P., Eisner, L., 2019. Phenology
868 and Magnitude of Primary Production in the Eastern Bering Sea, in: Siddon, E., Zador, S.
869 (Eds.), Ecosystem Status Report 2019: Eastern Bering Sea, Stock Assessment and Fishery
870 Evaluation Report. North Pacific Fishery Management Council, Anchorage, Alaska, United
871 States, pp. 67-70.
872 Olson, M.B., Strom, S.L., 2002. Phytoplankton growth, microzooplankton herbivory and
873 community structure in the southeast Bering Sea: insight into the formation and temporal
874 persistence of an Emiliania huxleyi bloom. Deep-Sea Res. II 49, 5969-5990.
875 Selph, K.E., Landry, M.R., Allen, C.B., Calbet, A., Christensen, S., Bidigare, R.R., 2001.
876 Microbial community composition and growth dynamics in the Antarctic Polar Front and
877 seasonal ice zone during late spring 1997. Deep-Sea Res. II 48, 4059-4080.
878 Sherr, E.B., Sherr, B.F., 2007. Heterotrophic dinoflagellates: a significant component of
879 microzooplankton biomass and major grazers of diatoms in the sea. Mar. Eco. Prog. Ser. 352,
880 187-197.
881 Sherr, E.B., Sherr, B.F., Hartz, A.J., 2009. Microzooplankton grazing impact in the Western
882 Arctic Ocean. Deep-Sea Res. II 56, 1264-1273.

Sherr, E.B., Sherr, B.F., Ross, C., 2013. Microzooplankton grazing impact in the Bering Sea during spring sea ice conditions. Deep-Sea Res. II 94, 57-67.
Spillane, T., 2016. Diatom Frustules as a Mechanical Defense Against Predation by Heterotrophic Dinoflagellates. Western Washington University, p. 51.
Stabeno, P.J., Farley Jr, E.V., Kachel, N.B., Moore, S., Mordy, C.W., Napp, J.M., Overland, J.E., Pinchuk, A.I., Sigler, M.F., 2012. A comparison of the physics of the northern and southern shelves of the eastern Bering Sea and some implications for the ecosystem. Deep-Sea Res. II 65, 14-30.
Stoecker, D.K., Weigel, A., Goes, J.I., 2014a. Microzooplankton grazing in the eastern Bering Sea in summer. Deep-Sea Res. II 109, 145-156.
Stoecker, D.K., Weigel, A.C., Stockwell, D.A., Lomas, M.W., 2014b. Microzooplankton: Abundance, biomass and contribution to chlorophyll in the Eastern Bering Sea in summer. Deep-Sea Res. II 109, 134-144.
Strom, S.L., Bright, K.J., Fredrickson, K.A., Cooney, E.C., 2017. Phytoplankton defenses: Do Emiliania huxleyi coccoliths protect against microzooplankton predators? Limnol. Oceanogr. 63, 617-627.
Strom, S.L., Fredrickson, K.A., 2008. Intense stratification leads to phytoplankton nutrient limitation and reduced microzooplankton grazing in the southeastern Bering Sea. Deep-Sea Res. II 55, 1761-1774.
Taniguchi, A., Saito, K., Koyama, A., Fukuchi, M., 1976. Phytoplankton communities in the Bering Sea and adjacent seas. J. Oceanogr. 32, 99-106.
Walsh, J.E., Thoman, R.L., Bhatt, U.S., Bieniek, P.A., Brettschneider, B., Brubaker, M., Danielson, S., Lader, R., Fetterer, F., Holderied, K., 2018. The high latitude marine heat wave of 2016 and its impacts on Alaska. B. Am. Meteorol. Soc. 99, S39-S43.
Yang, E.J., Ha, H.K., Kang, S.-H., 2015. Microzooplankton community structure and grazing impact on major phytoplankton in the Chukchi sea and the western Canada basin, Arctic ocean. Deep-Sea Res. II 120, 91-102.
Zhang, S., Liu, H., Ke, Y., Li, B., 2017. Effect of the silica content of diatoms on protozoan grazing. Front. Mar. Sci. 4, 202.

Fig. Captions

Fig. 1. ASGARD station map with subareas among domains (A) showing changes in sea-ice extent proportion (1 = 100% coverage) during April (B), May (C), and June (D) between 1980 through 2019 in the southeastern Bering Sea (bold line), northern Bering Sea (bold cyan line), and Chukchi Sea (gray dashed line) Seas; 2017 is highlighted (gray) in B, C, D. For reference, ASGARD 2017 stations are plotted on the map. Domain subareas (boxes) include southeastern Bering Sea (57.5 – 58.0° N, -168 – -162° E), northern Bering Sea (63.9 – 64.5° N, -172 – -166° E), and Chukchi Sea (70.0 – 70.5° N, -172 – -166° E). Data are from MERRA Data Assimilation model (GMAO, 2008) with 0.5° x 0.667° spatial- and 1-month temporal resolution and are averaged for each boxed region shown (map); accessed through Giovanni NASA EarthData version 4.33 (giovanni.gsfc.nasa.gov).

Fig. 2. Spatial distribution of properties in the upper (A – E) and lower (F – J) euphotic zone during ASGARD. (A, F) CTD-determined temperature, (B, G) nitrate, (C, H) ≥5 µm Chl *a*, (D, I) $bSiO_2$ and (E, J) diatom µ. For each property, the color bar under the lower-euphotic-zone panel applies to both light depths. Plots generated using Ocean Data View. Note: Transit station 1 not shown (see Table 1).

Fig. 3. Changes in the net increase in Chl *a* (d^{-1}) with percentage of whole seawater between ≥5 µm Chl *a* and <5 µm Chl *a* fractions at stations DBO3.8A at 3 m where both size fractions had non-zero slopes (A) and CNL3 at 4 m where only the <5 µm Chl *a* fraction had a non-zero slope (B). If significant, Model-I linear regressions are shown. These stations are representative of our typical responses (other stations in Supplemental Fig. 1), specifically that <5 µm Chl *a* samples had non-zero MZP grazing rates whereas a majority of MZP grazing rates in the ≥5 µm Chl *a* size fraction was zero.

Fig. 4. Diatom V_b and µ vs. dissolved silicic acid concentration (A, B, respectively), (C) diatom µ vs. nitrate concentration, and (D) diatom µ vs. temperature during ASGARD (upper euphotic zone, filled circles, and lower euphotic zone, gray circles) along with a prior CS field study (upward triangles) reporting diatom growth rates from dilution experiments (Yang et al., 2015) relative to the empirical relationship for phytoplankton growth and temperature (black line)

944 described by Eppley (1972). Error bars on A are SD. Geometric mean regressions and R^2 are
945 shown in B, C, with reported ANOVA F and p values. Point denoted by * not used in regressions
946 or ANCOVA analysis.
947
948 **Fig. 5.** Comparison of the frequency of dilution experiments where MZP grazing was zero (i.e.
949 not resolved) for previously published spring (Connell et al., 2018; Sherr et al., 2009; Sherr et al.,
950 2013) and summer (Liu et al., 2002; Olson and Strom, 2002; Sherr et al., 2009; Stoecker et al.,
951 2014a; Strom and Fredrickson, 2008; Yang et al., 2015) studies in the southeastern BS and CS
952 domains. Only summer studies reported size-fractionated rates. We compare our rates based on
953 total Chl *a* (sum of size fractions for our study, black bars) and the size-fractionated components
954 (≥5 µm light gray bars, <5 µm dark gray bars).
955
956 **Fig. 6.** A) Comparison of MZP grazing loss relative to phytoplankton µ ($g \times \mu^{-1}$) during bloom
957 and non-bloom conditions (mean ± SE to account for sample size differences). Open bars denote
958 average among all stations, regardless of whether MZP grazing was significantly different from
959 zero as in Sherr et al. (2013); hatched bars denote average when a value of 0 is applied for non-
960 significant grazing (i.e. reported $g \times \mu^{-1}$ averages in Results). B) The rate of diatom primary
961 productivity (PP) was converted using Si:C for cold-adapted diatoms (Lomas et al., 2019), also
962 shown is the quantity of diatom PP which escapes MZP grazing (calculated as PP x $(1 - (g \times \mu^{-1}))$
963 $^{1}))$ for bloom and non-bloom conditions. Open and hatched bars denote using $g \times \mu^{-1}$ averages as
964 described for panel A. SE in panel B were propagated from ($g \times \mu^{-1}$) and ρ error terms.

Table 1: Hydrography, nutrients (µM), size-fractionated Chl *a* (µg L^{-1}), $bSiO_2$ standing stock (µmol Si L^{-1}) and that associated with only living diatoms (Live $bSiO_2$ as % of total $bSiO_2$) for the ASGARD cruise and pre-cruise transit ("Transit" stations) from the southeastern BS to Nome, Alaska. Error term is SD (n = 3). "--" indicate no data.

Station #	Date (DD-Month-YY)	Lat. (°N)	Long (°E)	Depth (m)	T (°C)	$Si(OH)_4$ (µM)	SRP (µM)	NO_3^- (µM)	NH_4^+ (µM)	≥5 µm Chl *a* (µg L^{-1})	<5 µm Chl *a* (µg L^{-1})	$bSiO_2$ (µmol Si L^{-1})	Live $bSiO_2$ (%)
Transit 1	05-Jun-17	56.39	-167.15	35	4.00	2.9	0.61	1.5	1.55	--	--	0.10 ± 0.01	--
Transit 2	06-Jun-17	60.44	-168.20	5	3.18	0.5	0.88	0.0	0.05	0.81 ± 0.14	0.05 ± 0.03	4.32 ± 0.93	39%
				24	3.02	0.7	0.89	0.0	0.03	1.81 ± 0.12	0.02 ± 0.02	7.10 ± 0.11	--
Transit 3	07-Jun-17	64.27	-165.71	5	2.39	1.7	0.87	0.1	0.09	0.20 ± 0.02	--	3.86 ± 0.17	7%
				10	0.30	1.8	0.99	0.1	0.23	0.35 ± 0.03	0.03 ± 0.02	6.24 ± 0.66	4%
CBE9	09-Jun-17	64.38	-167.07	5	4.22	2.1	0.49	0.1	0.27	0.07 ± 0.01	0.19 ± 0.01	0.99 ± 0.05	316%
				26	-0.44	4.2	0.96	0.5	1.09	1.15 ± 0.91	0.46 ± 0.02	8.44 ± 0.33	--
CBW5	11-Jun-17	64.15	-171.51	7	6.54	5.9	0.49	3.1	0.46	0.07 ± 0.00	0.23 ± 0.03	0.54 ± 0.02	--
				29	1.60	28.5	1.81	17.9	1.61	0.23 ± 0.06	0.07 ± 0.02	6.87 ± 0.38	2%
CNL3	13-Jun-17	66.50	-168.96	4	5.59	1.9	0.28	0.0	0.06	0.40 ± 0.02	0.13 ± 0.03	1.98 ± 0.04	105%
				18	2.17	5.9	1.02	6.6	1.81	4.70 ± 1.14	0.10 ± 0.04	15.2 ± 0.4	72%
IL2	14-Jun-17	67.54	-164.88	5	4.71	1.6	0.40	0.0	0.00	--	--	0.66 ± 0.07	13%
				33	-1.22	11.8	0.99	2.0	0.46	--	--	13.6 ± 0.1	92%
DBO3.8A	15-Jun-17	67.67	-168.73	3	2.70	11.9	1.21	9.2	1.06	4.99 ± 0.89	0.15 ± 0.04	13.9 ± 0.1	42%
				13	2.30	11.7	1.22	9.5	1.16	4.71 ± 0.23	0.18 ± 0.03	13.8 ± 2.3	70%
DBO3.3	16-Jun-17	68.18	-167.31	5	6.14	0.9	0.49	0.0	0.02	0.11 ± 0.04	0.23 ± 0.01	0.76 ± 0.46	30%
				22	1.55	1.6	0.72	0.1	1.26	0.40 ± 0.01	0.23 ± 0.10	3.51 ± 0.19	28%
CL3	17-Jun-17	69.03	-168.89	6	6.17	0.7	0.56	0.1	0.35	0.13 ± 0.02	0.20 ± 0.00	1.48 ± 0.03	23%
				22	2.36	4.7	1.15	3.2	4.40	0.30 ± 0.12	0.05 ± 0.00	7.64 ± 0.97	8%
CL1	18-Jun-17	68.95	-166.91	5	2.63	5.4	0.68	0.2	0.37	0.08 ± 0.02	0.31 ± 0.07	0.95 ± 0.01	5%
				22	0.33	4.1	0.81	0.9	1.34	0.35 ± 0.03	0.30 ± 0.05	1.85 ± 0.04	14%
DBO3.8	20-Jun-17	67.67	-168.96	4	3.87	3.7	0.47	0.6	0.06	16.45 ± 2.19	0.39 ± 0.13	14.5 ± 0.1	165%
				17	3.87	5.8	0.61	2.7	0.59	17.57 ± 2.42	0.36 ± 0.07	14.0 ± 0.2	190%
IL4	21-Jun-17	67.41	-165.79	5	4.07	1.6	0.55	0.2	0.86	0.22 ± 0.03	0.26 ± 0.02	1.91 ± 0.08	9%
				22	3.24	2.4	0.67	0.3	1.66	0.17 ± 0.02	0.24 ± 0.05	2.75 ± 0.11	7%
CPL 6	22-Jun-17	66.50	-167.70	4	2.95	2.1	0.65	0.1	0.89	0.46 ± 0.02	0.57 ± 0.06	4.28 ± 0.10	6%
				16	2.89	2.4	0.62	0.2	0.94	0.40 ± 0.03	0.55 ± 0.01	3.93 ± 0.02	--
DBO2.4	24-Jun-17	64.96	-169.89	5	2.66	31.4	1.69	16.7	1.52	0.47 ± 0.09	0.36 ± 0.11	10.3 ± 1.1	4%
				21	2.66	33.4	1.67	17.6	1.62	0.48 ± 0.23	0.30 ± 0.06	10.8 ± 1.7	3%
DBO2.2	26-Jun-17	64.68	-169.10	4	3.40	29.8	1.54	15.9	0.29	1.53 ± 0.17	1.09 ± 0.34	6.65 ± 0.18	25%
				17	2.87	30.6	1.62	16.9	0.78	1.99 ± 0.62	0.82 ± 0.10	7.41 ± 0.31	17%

Table 2 – ^{32}Si-based rate measurements: biogenic silica production, ρ (µmol Si L^{-1} d^{-1}), total $bSiO_2$-normalized production, V_b (d^{-1}), diatom growth, µ (d^{-1}); ± SD. Dilution based rate measurements: MZP grazing rates, g (d^{-1}) and phytoplankton growth rate, µ (d^{-1}) among size fractions (≥5 µm, <5 µm); mean ± SE of the regression fit, p-value for the regression fit is in parentheses. Abbreviations are "ns" (not significant) and "--" (no data). *Denotes V_b = diatom µ as "Live" $bSiO_2$ (FlowCam derived) exceeded 100% of total $bSiO_2$. As in Sherr et al. (2013) the g μ^{-1} calculation for each experiment is done regardless of whether grazing is significant. †Denotes 0% when grazing was negative (i.e. below detection) or 100% when phytoplankton µ was negative and grazing positive.

Station #	Depth (m)	ρ (µmol Si L^{-1} d^{-1})	V_b (d^{-1})	diatom µ (d^{-1})	≥5 µm g (d^{-1}), p-value	≥5 µm µ (d^{-1}), p-value	≥5 µm g μ^{-1} (%)	<5 µm g (d^{-1}), p-value	<5 µm µ (d^{-1}), p-value	<5 µm g μ^{-1} (%)
Transit 1	35	<0.00 ± <0.00	0.01 ± <0.00	--	--	--	--	--	--	--
Transit 2	5	0.10 ± 0.02	0.02 ± <0.00	0.06	0.81 ± 0.48 (0.03)	1.06 ± 0.48 (ns)	76	-1.94 ± 1.36 (0.03)	-2.68 ± 1.36 (ns)	†0
Transit 2	24	0.22 ± 0.01	0.03 ± <0.00	--	0.34 ± 0.11 (0.04)	0.17 ± 0.11 (0.01)	199	0.82 ± 0.34 (ns)	-0.41 ± 0.34 (0.04)	†100
Transit 3	5	0.08 ± <0.00	0.01 ± 0.01	0.30	0.54 ± 0.30 (ns)	0.28 ± 0.30 (ns)	195	--	--	--
Transit 3	10	0.19 ± 0.05	0.03 ± 0.01	0.79	-0.32 ± 0.84 (ns)	-0.50 ± 0.84 (ns)	†0	-0.80 ± 0.58 (ns)	0.751 ± 0.58 (ns)	†0
CBE9	5	0.02 ± <0.01	0.02 ± <0.01	*0.02	0.53 ± 0.25 (ns)	-0.07 ± 0.25 (ns)	†100	0.61 ± 0.09 (<0.01)	0.35 ± 0.09 (<0.01)	175
CBE9	26	0.10 ± 0.02	0.01 ± <0.01	--	-0.00 ± 0.17 (<0.01)	0.61 ± 0.17 (ns)	†0	0.68 ± 0.16 (<0.01)	0.46 ± 0.16 (<0.01)	147
CBW5	7	0.05 ± <0.01	0.10 ± <0.01	--	0.15 ± 0.40 (ns)	0.10 ± 0.40 (ns)	142	0.36 ± 0.07 (<0.01)	0.49 ± 0.07 (<0.01)	74
CBW5	29	0.02 ± <0.01	<0.01 ± <0.01	0.13	-0.39 ± 0.20 (ns)	-0.35 ± 0.20 (ns)	†0	0.33 ± 0.15 (<0.01)	0.56 ± 0.15 (ns)	†100

CNL3	4	0.10 ± 0.01	0.05 ± <0.01	*0.05	0.57 ± 0.10 (0.02)	0.18 ± 0.10 (<0.01)	314	1.65 ± 0.35 (<0.01)	0.83 ± 0.35 (<0.01)	197
CNL3	18	1.07 ± 0.19	0.07 ± 0.01	0.09	0.41 ± 0.67 (ns)	-0.18 ± 0.67 (ns)	†100	0.46 ± 0.14 (<0.01)	0.65 ± 0.14 (<0.01)	71
DBO3.8A	3	1.81 ± 0.04	0.12 ± <0.01	0.29	-0.06 ± 0.64 (ns)	0.01 ± 0.64 (ns)	†0	0.44 ± 0.13 (<0.01)	0.47 ± 0.13 (<0.01)	96
DBO3.8A	13	2.03 ± 0.10	0.14 ± <0.01	0.20	0.42 ± 0.22 (<0.01)	1.23 ± 0.22 (ns)	34	0.66 ± 0.18 (<0.01)	1.09 ± 0.18 (<0.01)	61
DBO3.3	5	0.02 ± <0.01	0.03 ± <0.01	0.09	3.33 ± 0.87 (0.03)	1.39 ± 0.87 (<0.01)	239	2.70 ± 0.85 (<0.01)	1.99 ± 0.85 (0.01)	136
DBO3.3	22	0.09 ± <0.01	0.03 ± <0.01	0.09	-0.06 ± 0.09 (ns)	-0.06 ± 0.09 (ns)	†0	0.46 ± 0.08 (<0.01)	0.61 ± 0.08 (<0.01)	75
CL3	6	0.02 ± <0.01	0.01 ± <0.01	0.05	-0.17 ± 0.11 (<0.01)	-0.67 ± 0.11 (ns)	†0	0.28 ± 0.05 (<0.01)	0.63 ± 0.05 (<0.01)	45
CL3	22	0.03 ± <0.01	<0.01 ± <0.01	0.05	2.94 ± 0.56 (0.02)	0.99 ± 0.56 (<0.01)	295	2.29 ± 0.51 (<0.01)	1.77 ± 0.51 (<0.01)	130
CL1	5	0.01 ± <0.01	<0.01 ± <0.01	0.18	-0.79 ± 0.09 (<0.01)	-0.50 ± 0.09 (<0.01)	†0	0.49 ± 0.18 (<0.01)	0.40 ± 0.18 (0.02)	123
CL1	22	0.02 ± <0.01	<0.01 ± <0.01	0.06	0.34 ± 0.10 (ns)	-0.09 ± 0.10 (<0.01)	†100	0.50 ± 0.10 (<0.01)	0.40 ± 0.10 (<0.01)	123
DBO3.8 bloom	4	1.19 ± 0.21	0.08 ± 0.01	*0.08	0.01 ± 0.15 (<0.01)	0.58 ± 0.15 (ns)	2	0.49 ± 0.17 (ns)	0.16 ± 0.17 (0.01)	†0
DBO3.8 bloom	17	1.57 ± 0.26	0.11 ± 0.02	*0.11	0.49 ± 0.23 (<0.01)	0.61 ± 0.23 (ns)	81	0.54 ± 0.07 (<0.01)	0.59 ± 0.07 (<0.01)	91

IL4	5	0.03 ± <0.01	0.02 ± <0.01	0.18	-0.52 ± 0.16 (ns)	-0.26 ± 0.16 (0.01)	†0	0.02 ± 0.13 (<0.01)	0.48 ± 0.13 (ns)	†100
IL4	22	0.01 ± <0.01	<0.01 ± <0.01	0.06	-0.71 ± 0.90 (ns)	-0.66 ± 0.90 (ns)	†0	0.09 ± 0.34 (ns)	-0.06 ± 0.34 (ns)	†100
CPL 6	4	0.05 ± <0.01	0.01 ± <0.01	0.21	0.12 ± 0.19 (ns)	-0.13 ± 0.19 (ns)	†100	0.78 ± 0.13 (<0.01)	0.84 ± 0.13 (<0.01)	92
CPL 6	16	0.04 ± <0.01	<0.01 ± <0.01	--	0.06 ± 0.15 (ns)	-0.21 ± 0.15 (ns)	†100	0.46 ± 0.05 (<0.01)	0.34 ± 0.05 (<0.01)	134
DBO2.4	5	0.18 ± <0.01	0.02 ± <0.01	0.47	0.20 ± 0.20 (<0.01)	0.63 ± 0.20 (ns)	33	-0.22 ± 0.10 (<0.01)	0.08 ± 0.10 (<0.01)	†0
DBO2.4	21	0.04 ± <0.01	<0.01 ± <0.01	0.12	-0.60 ± 0.23 (ns)	0.15 ± 0.23 (0.02)	†0	0.86 ± 0.14 (<0.01)	0.75 ± 0.14 (<0.01)	114
DBO2.2	4	1.21 ± 0.10	0.17 ± 0.01	0.68	-0.49 ± 0.19 (<0.01)	0.50 ± 0.19 (0.02)	†0	0.70 ± 0.39 (0.03)	0.82 ± 0.39 (ns)	†100
DBO2.2	17	0.22 ± 0.02	0.03 ± <0.01	0.17	0.15 ± 0.11 (<0.01)	-0.30 ± 0.11 (ns)	†100	0.69 ± 0.14 (<0.01)	0.63 ± 0.14 (<0.01)	109

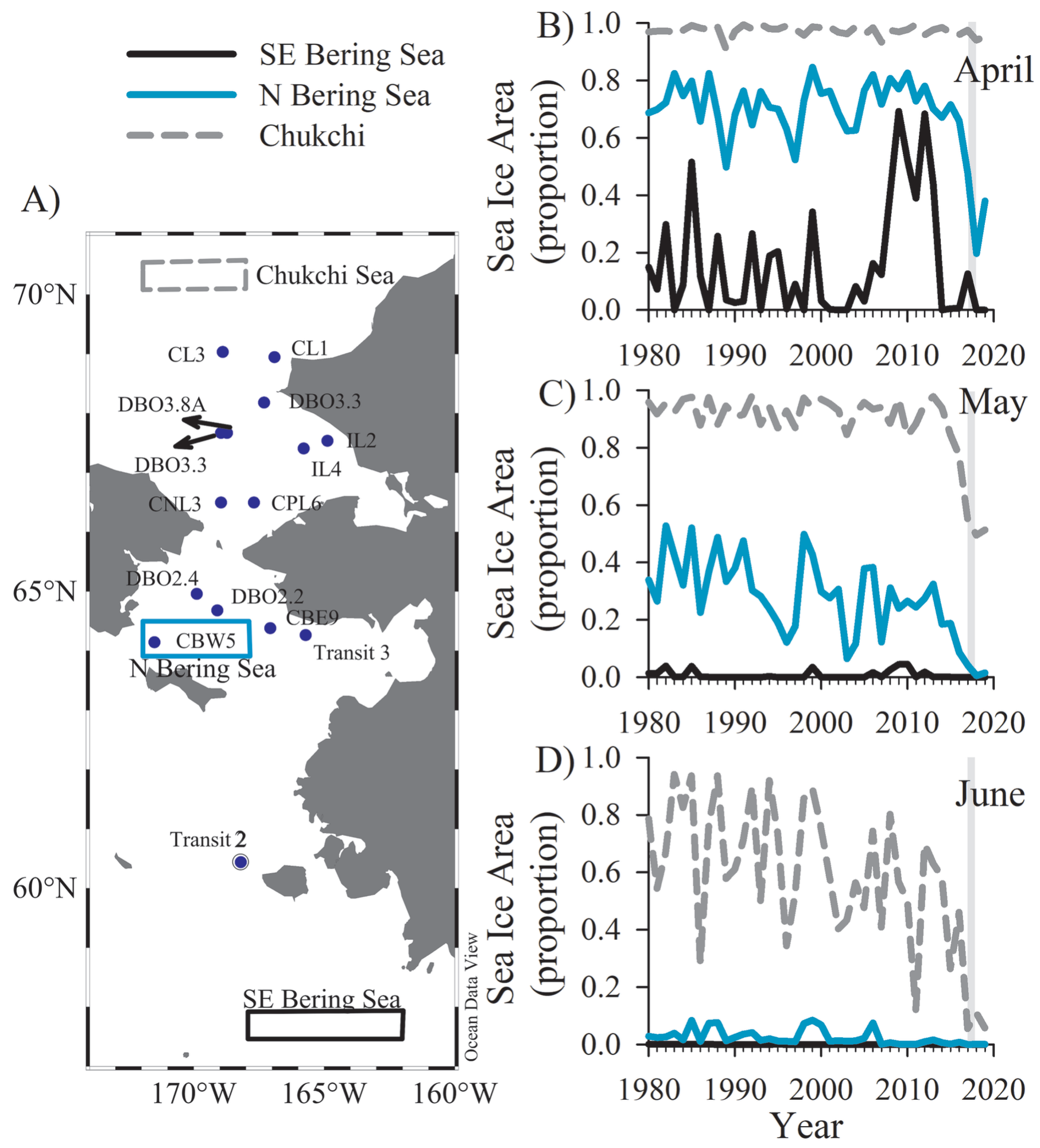
SE Bering Sea
N Bering Sea
Chukchi
A)
Chukchi Sea
70°N
65°N
60°N
CL3
CL1
DBO3.8A
DBO3.3
IL2
DBO3.3
IL4
CNL3
CPL6
DBO2.4
DBO2.2
CBE9
CBW5
Transit 3
N Bering Sea
Transit 2
SE Bering Sea
170°W
165°W
160°W
Ocean Data View
B)
April
C)
May
D)
June
Sea Ice Area (proportion)
1.0
0.8
0.6
0.4
0.2
0.0
1980
1990
2000
2010
2020
Year

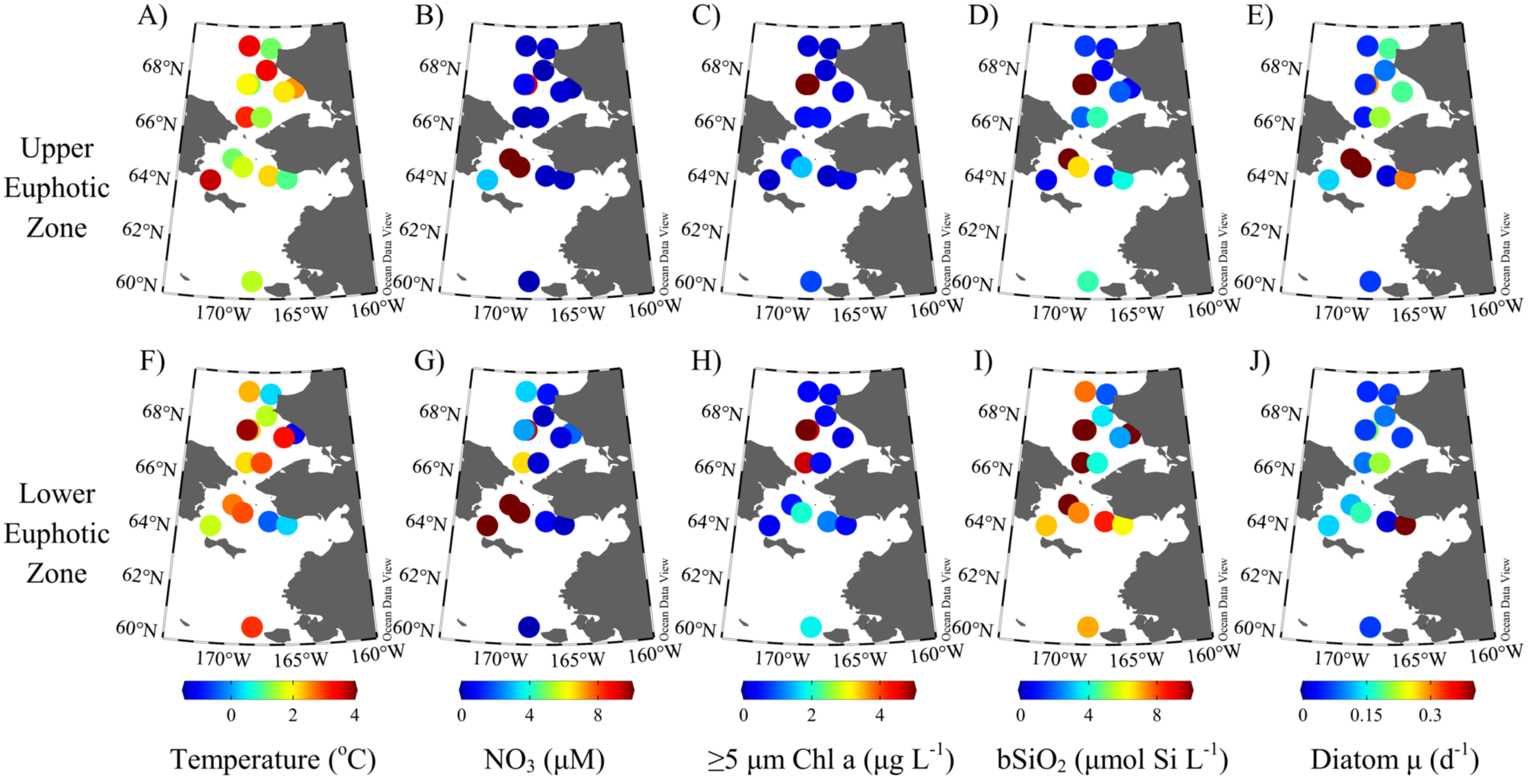
A)
B)
C)
D)
E)
F)
G)
H)
I)
J)
Upper Euphotic Zone
Lower Euphotic Zone
68°N
66°N
64°N
62°N
60°N
170°W
165°W
160°W
Ocean Data View
0
2
4
Temperature (°C)
0
4
8
NO3 (µM)
0
2
4
≥5 µm Chl a (µg L-1)
0
4
8
bSiO2 (µmol Si L-1)
0
0.15
0.3
Diatom µ (d-1)

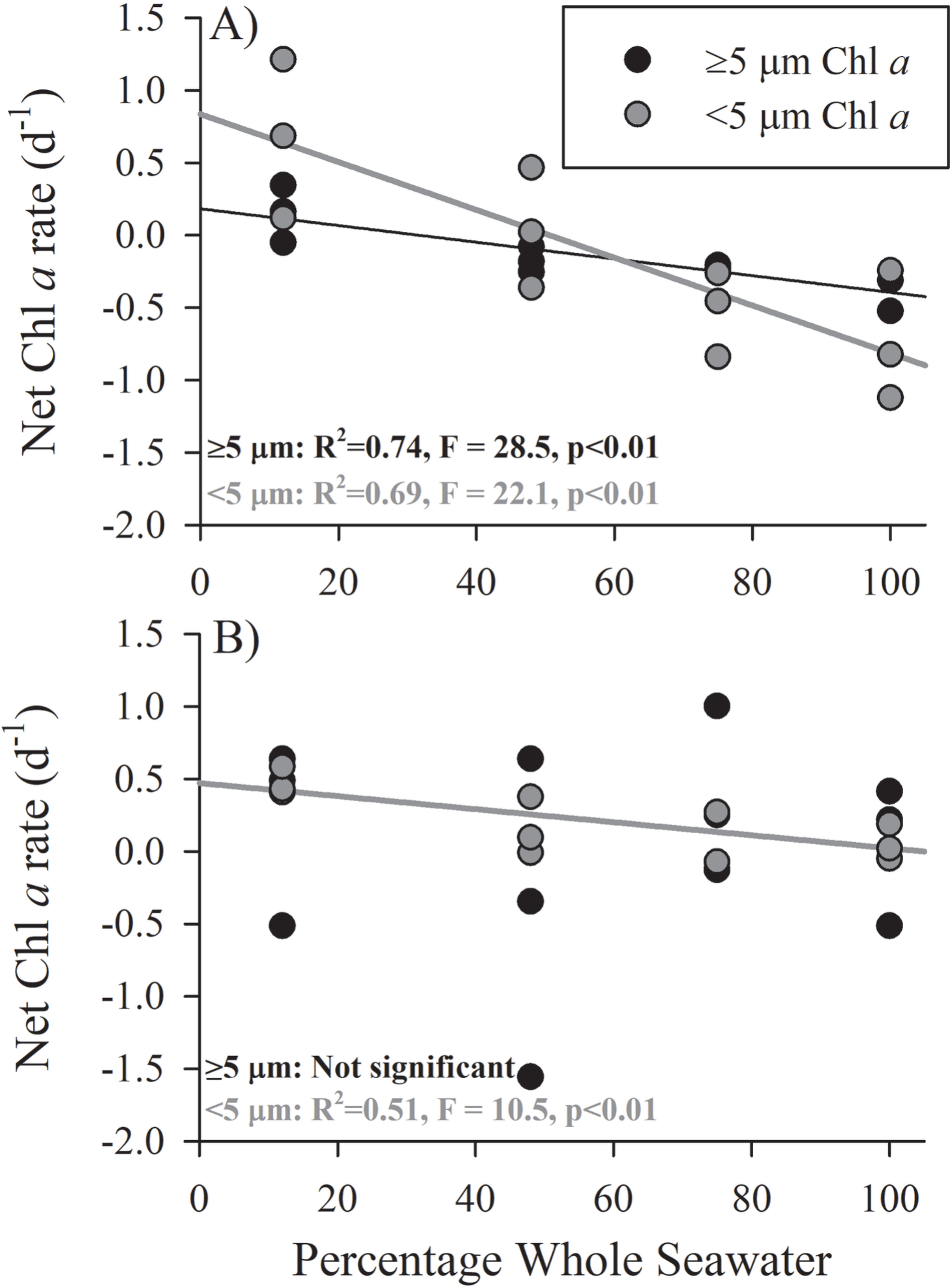
A)
B)
≥5 µm Chl a
<5 µm Chl a
Net Chl a rate (d-1)
≥5 µm: R2=0.74, F = 28.5, p<0.01
<5 µm: R2=0.69, F = 22.1, p<0.01
≥5 µm: Not significant
<5 µm: R2=0.51, F = 10.5, p<0.01
1.5
1.0
0.5
0.0
-0.5
-1.0
-1.5
-2.0
0
20
40
60
80
100
Percentage Whole Seawater

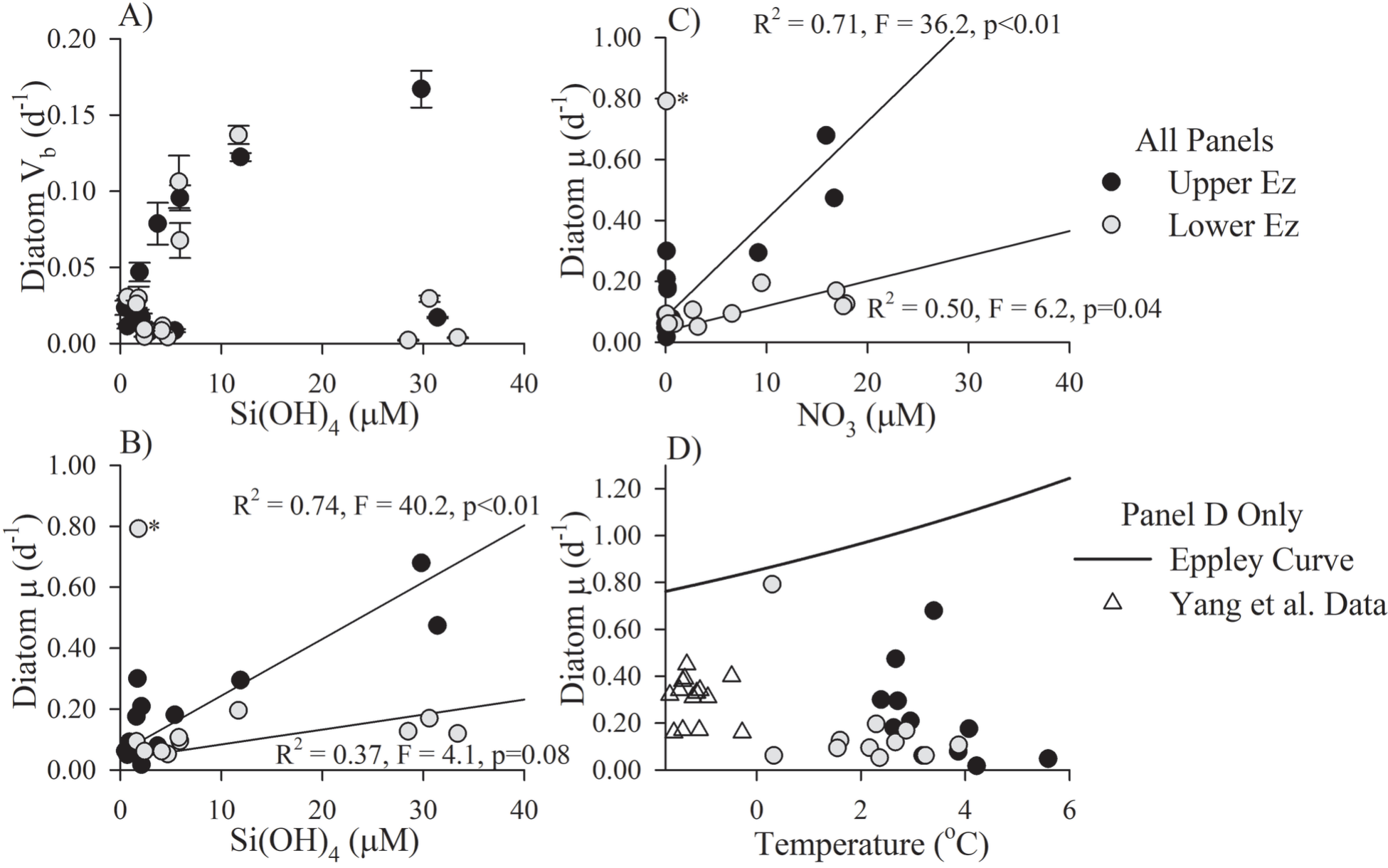
A)
Diatom V_b (d^{-1})
0.20
0.15
0.10
0.05
0.00
0
10
20
30
40
$Si(OH)_4$ (µM)
B)
Diatom µ (d^{-1})
1.00
0.80
0.60
0.40
0.20
0.00
*
R^2 = 0.74, F = 40.2, p<0.01
R^2 = 0.37, F = 4.1, p=0.08
0
10
20
30
40
$Si(OH)_4$ (µM)
C)
Diatom µ (d^{-1})
1.00
0.80
0.60
0.40
0.20
0.00
*
R^2 = 0.71, F = 36.2, p<0.01
R^2 = 0.50, F = 6.2, p=0.04
0
10
20
30
40
NO_3 (µM)
D)
Diatom µ (d^{-1})
1.20
1.00
0.80
0.60
0.40
0.20
0.00
0
2
4
6
Temperature (^oC)
All Panels
Upper Ez
Lower Ez
Panel D Only
Eppley Curve
Yang et al. Data

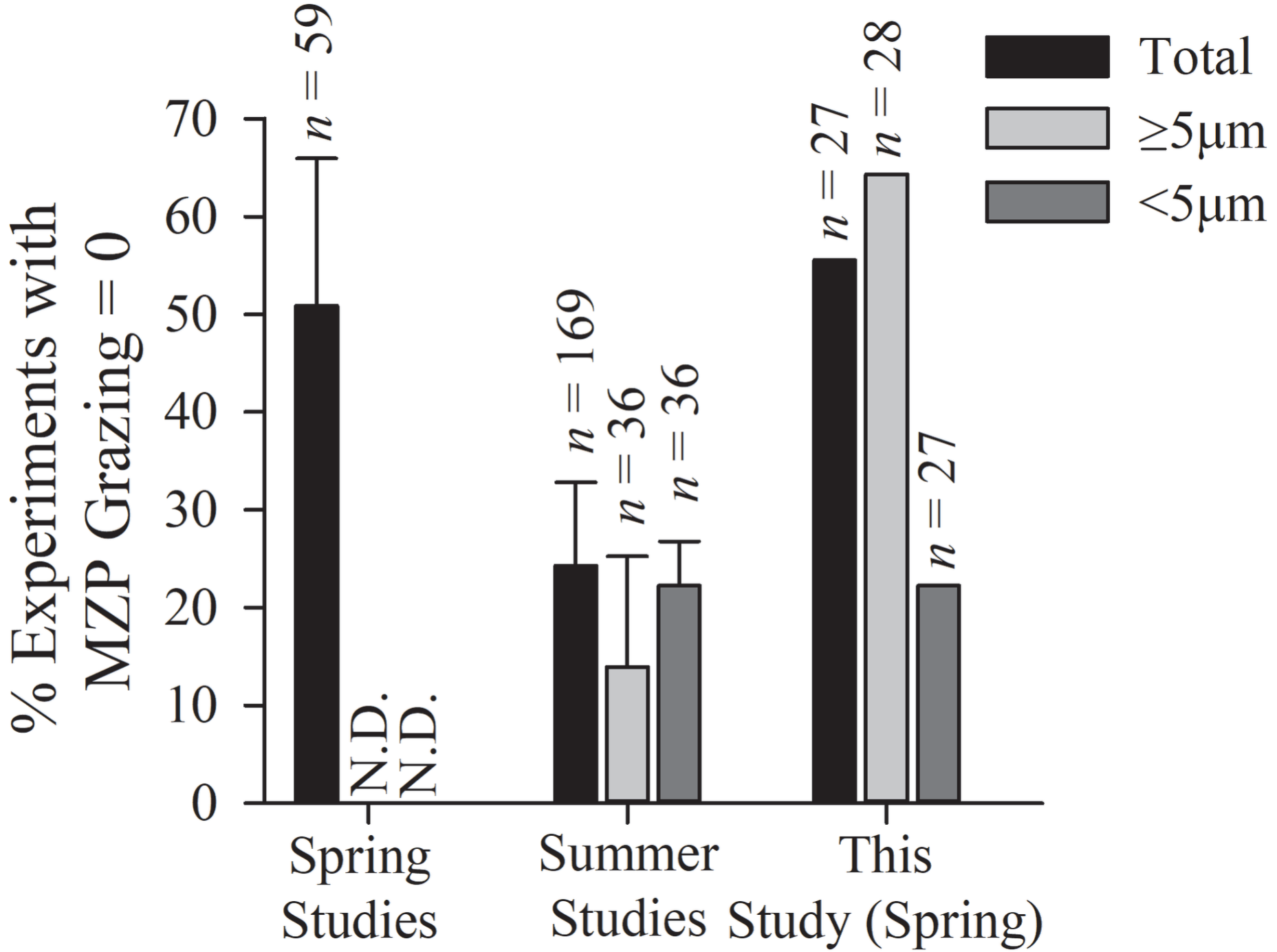
% Experiments with MZP Grazing = 0
70
60
50
40
30
20
10
0
n = 59
N.D.
N.D.
n = 169
n = 36
n = 36
n = 27
n = 28
n = 27
Total
≥5µm
<5µm
Spring Studies
Summer Studies
This Study (Spring)

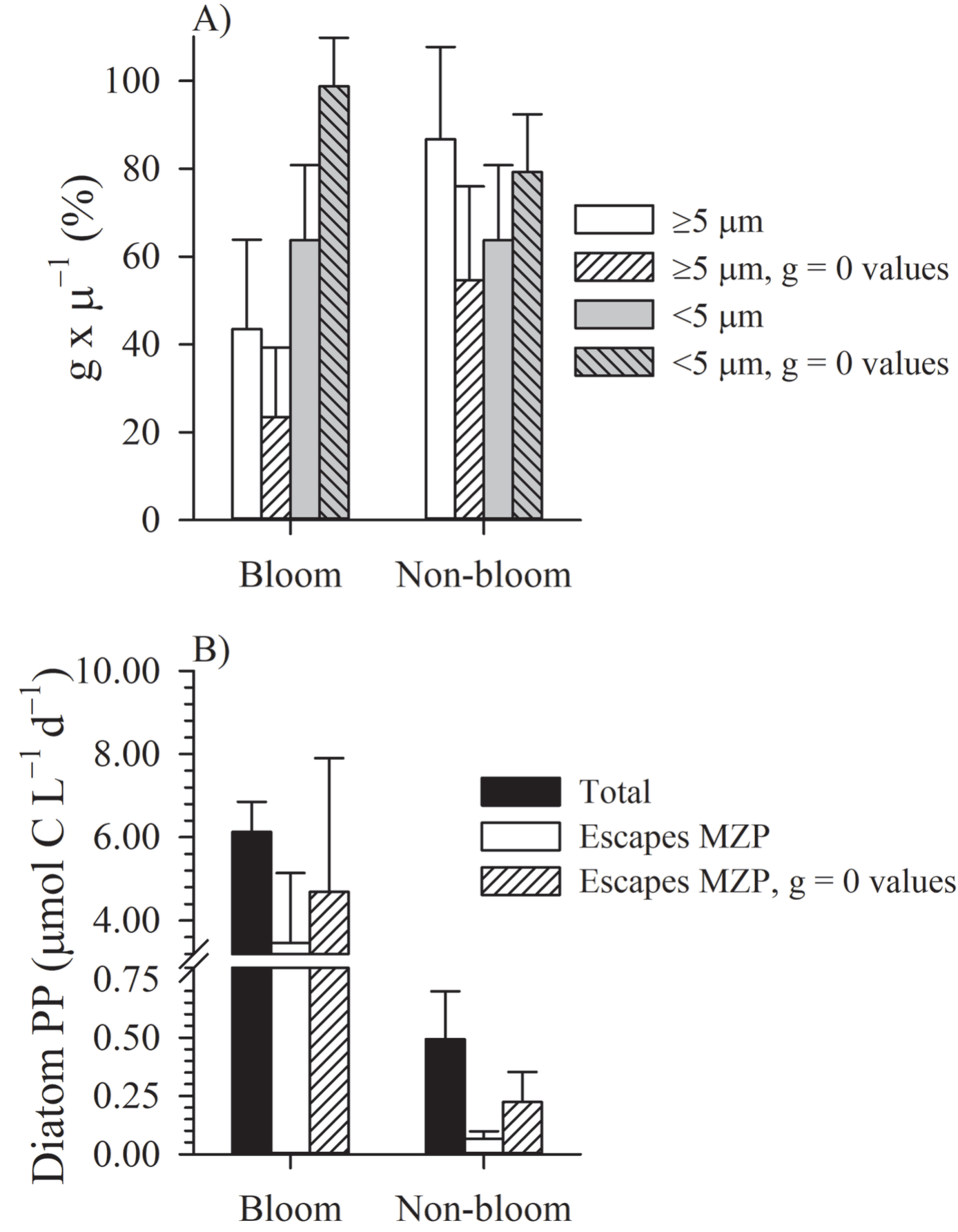
A)
100
80
60
40
20
0
g x μ⁻¹ (%)
≥5 μm
≥5 μm, g = 0 values
<5 μm
<5 μm, g = 0 values
Bloom
Non-bloom
B)
10.00
8.00
6.00
4.00
0.75
0.50
0.25
0.00
Diatom PP (μmol C L⁻¹ d⁻¹)
Total
Escapes MZP
Escapes MZP, g = 0 values
Bloom
Non-bloom